NAVAL POSTGRADUATE SCHOOL

MONTEREY, CALIFORNIA

THESIS

EVALUATION OF COMPOSITE-HULL SHIPS OPERATING IN ARCTIC ICE

by

Ryan M. Tran

June 2016

Thesis Advisor: Young W. Kwon
Co-Advisor: Jarema M. Didoszak

Approved for public release; distribution is unlimited

THIS PAGE INTENTIONALLY LEFT BLANK

REPORT DOCUMENTATION PAGE			*Form Approved OMB No. 0704–0188*
Public reporting burden for this collection of information is estimated to average 1 hour per response, including the time for reviewing instruction, searching existing data sources, gathering and maintaining the data needed, and completing and reviewing the collection of information. Send comments regarding this burden estimate or any other aspect of this collection of information, including suggestions for reducing this burden, to Washington headquarters Services, Directorate for Information Operations and Reports, 1215 Jefferson Davis Highway, Suite 1204, Arlington, VA 22202-4302, and to the Office of Management and Budget, Paperwork Reduction Project (0704-0188) Washington, DC 20503.			
1. AGENCY USE ONLY ***(Leave blank)***	**2. REPORT DATE** June 2016	**3. REPORT TYPE AND DATES COVERED** Master's thesis	
4. TITLE AND SUBTITLE EVALUATION OF COMPOSITE-HULL SHIPS OPERATING IN ARCTIC ICE		**5. FUNDING NUMBERS**	
6. AUTHOR Ryan M. Tran			
7. PERFORMING ORGANIZATION NAME(S) AND ADDRESS(ES) Naval Postgraduate School Monterey, CA 93943-5000		**8. PERFORMING ORGANIZATION REPORT NUMBER**	
9. SPONSORING /MONITORING AGENCY NAME(S) AND ADDRESS(ES) N/A		**10. SPONSORING / MONITORING AGENCY REPORT NUMBER**	
11. SUPPLEMENTARY NOTES The views expressed in this thesis are those of the author and do not reflect the official policy or position of the Department of Defense or the U.S. Government. IRB Protocol number ____N/A____.			
12 a. DISTRIBUTION / AVAILABILITY STATEMENT Approved for public release; distribution is unlimited		**12 b. DISTRIBUTION CODE**	

13. ABSTRACT (maximum 200 words)

As ocean temperatures rise, naval exploration around the Arctic Ocean is increasing due to the rapidly melting ice caps. Extensive research is thus being conducted to determine the interaction between ice and steel-hulls in anticipation of opening sea lanes. While the majority of the research focuses on traditional steel-hull ships, limited research has been conducted on composite-hull ships to determine how this material will respond in Arctic waters. Therefore, the purpose of this study is to evaluate how composite materials interact with free-floating ice. The program, DYSMAS, conducted a computational parametric analysis to determine how increasing ship velocity, expanding ice block size, adding ice blocks, and changing the hull shape (vertical, tumblehome, and flared) affected the ship's performance. The numerical tests reveal that the ice block position has the greatest influence on the effective stress for the ship. Additionally, a second component of this thesis was to design and build a wave generating system. The system was designed and partially built, but an unexpected closure prevented the completion of construction. This project provides the foundation for both experimental and computational research relevant to composite-hull ships transiting through ice fields.

14. SUBJECT TERMS composite, ships, Arctic, sea ice, DYSMAS, wave generator, plunger			**15. NUMBER OF PAGES** 117
			16. PRICE CODE
17. SECURITY CLASSIFICATION OF REPORT Unclassified	**18. SECURITY CLASSIFICATION OF THIS PAGE** Unclassified	**19. SECURITY CLASSIFICATION OF ABSTRACT** Unclassified	**20. LIMITATION OF ABSTRACT** UU

NSN 7540–01-280-5500 Standard Form 298 (Rev. 2–89)
Prescribed by ANSI Std. 239–18

THIS PAGE INTENTIONALLY LEFT BLANK

Approved for public release; distribution is unlimited

EVALUATION OF COMPOSITE-HULL SHIPS OPERATING IN ARCTIC ICE

Ryan M. Tran
Ensign, United States Navy
B.S., United States Naval Academy, 2015

Submitted in partial fulfillment of the
requirements for the degree of

MASTER OF SCIENCE IN MECHANICAL ENGINEERING

from the

NAVAL POSTGRADUATE SCHOOL
June 2016

Approved by: Young W. Kwon
Thesis Advisor

Jarema M. Didoszak
Co-Advisor

Garth V. Hobson
Chair, Department of Mechanical and Aerospace Engineering

THIS PAGE INTENTIONALLY LEFT BLANK

ABSTRACT

As ocean temperatures rise, naval exploration around the Arctic Ocean is increasing due to the rapidly melting ice caps. Extensive research is thus being conducted to determine the interaction between ice and steel-hulls in anticipation of opening sea lanes. While the majority of the research focuses on traditional steel-hull ships, limited research has been conducted on composite-hull ships to determine how this material will respond in Arctic waters. Therefore, the purpose of this study is to evaluate how composite materials interact with free-floating ice. The program, DYSMAS, conducted a computational parametric analysis to determine how increasing ship velocity, expanding ice block size, adding ice blocks, and changing the hull shape (vertical, tumblehome, and flared) affected the ship's performance. The numerical tests reveal that the ice block position has the greatest influence on the effective stress for the ship. Additionally, a second component of this thesis was to design and build a wave generating system. The system was designed and partially built, but an unexpected closure prevented the completion of construction. This project provides the foundation for both experimental and computational research relevant to composite-hull ships transiting through ice fields.

THIS PAGE INTENTIONALLY LEFT BLANK

TABLE OF CONTENTS

LIST OF FIGURES

THIS PAGE INTENTIONALLY LEFT BLANK

LIST OF TABLES

THIS PAGE INTENTIONALLY LEFT BLANK

ACKNOWLEDGMENTS

I would like to thank both of my thesis advisors, Professor Kwon and Professor Didoszak. Their guidance and dedication toward my thesis has allowed me to further develop as a student and military officer. I would not have succeeded at the Naval Postgraduate School without their mentorship. I am grateful to John Zseleczky for his willingness to help me design and build a wave tank. He guided me through the design process and shared his wave-generating system blueprints of the sediment tank at the U.S. Naval Academy. It was a pleasure working with Stefan Kohlgrueber, John Mobley and Levi Owe, who helped me build the wave-generating system. Raleigh Nielsen, from ModuSystems, helped me with the mechanical design for the wave tank. I would also like to thank Marianne Traflinger for reviewing and editing my thesis. Lastly, I thank my office partner, Jean Loomis, for working closely with me and helping me diagnose issues with the DYSMAS simulations.

THIS PAGE INTENTIONALLY LEFT BLANK

I. INTRODUCTION

As ocean temperatures rise, naval exploration around the Arctic Ocean is increasing due to the rapidly melting ice caps. An increase in travel primarily occurs during the summer shipping season, particularly through the Northwest Passage. The Northwest Passage connects the Atlantic and Pacific Oceans together through the Canadian Arctic Archipelago, shown in Figure 1. The passage is estimated to reduce the voyage distance between Japan and Northern Europe by 40% [1].

Figure 1. Northwest Passage. Source: [2].

Arctic sea ice has drastically decreased and become thinner over the past few decades, but studies suggest that the mean thickness is still over 3 m [3]. Therefore, research casts doubt that these sea lanes will be used for commercial shipping in the near future [2]. Regardless, extensive research is being conducted in anticipation of these sea lanes to determine the interaction between ice and steel-hulls. While the majority of the research focuses on traditional steel-hull ships, limited research has been conducted on composite-hull ships to determine how this material will operate in Arctic waters.

The purpose of this study was to evaluate how composite materials interact with free-floating ice. The computational analysis was completed in DYSMAS, a Department

of Defense program, and the experimental tests were performed in the tow tank at the Naval Postgraduate School (NPS). The NPS tow tank did not have any wave generating system; therefore, a second component of the thesis was to design and construct a wave maker. The goal was to analyze the project computationally and to build a wave tank for future experimental research.

A. BACKGROUND

The background section discusses the significance of researching composite materials in Arctic conditions. General information will be provided about Arctic stakeholders and how the region is pertinent to the United States. Furthermore, ship hulls and composite materials will be discussed. This thesis also presents prior research related to ships operating in Arctic conditions.

1. Arctic Stakeholders

Many parts of the Arctic are unknown due to the thick ice features that inhibit countries from exploring the region. As the oceans are warming, the Arctic ice is becoming thinner, and thus many countries and maritime industries are devoting resources to research and understand naval activity there. The Arctic features abundant oil supplies, gas, minerals, and shortened shipping routes. This economic opportunity has resulted in a global competition for influence in the region. Figure 2 illustrates the countries with territorial claims to the Arctic region.

Figure 2. Arctic Nations. Source: [4].

In 1991, the Arctic Council formed as an intergovernmental forum that addresses issues faced by Arctic governments and the indigenous people in the region [5]. The eight members of the Arctic Council are Canada, Denmark, Finland, Iceland, Norway, Russia, Sweden, and the United States. Twelve non-arctic countries have also been admitted as observers to the council, including France, Germany, the United Kingdom, Singapore, India, and China. These nations have sought opportunities in the region, and their participation as observers has allowed them to influence the decisions of the permanent eight council members [6]. The additional observers strengthen the Arctic Council because it demonstrate international acceptance [6].

2. U.S. Naval Significance

President Obama recognized the potential of this passage and called for the United States to increase its fleet of icebreakers [2]. In 2013, the U.S. Department of Defense published the Arctic Strategy, which outlines the Department's desire to create a "secure and stable region where U.S. national interests are safeguarded, the U.S. homeland is protected, and nations work cooperatively to address challenges" [7]. In

addition to policy, the Navy has been active in the longstanding training exercise, ICEX, which occurs every three years to develop and hone submarine operation warfighting capabilities in the Arctic environment [8]. Ships have traditionally sailed in warmer oceans and with this new frontier, new materials are being developed for ship hulls to efficiently operate in Arctic conditions.

3. Ship Hulls

The U.S. Navy has conducted extensive research on the interaction between steel-hulls and ice. Conventional steel-hulls, illustrated in Figure 3, have been a standard for many naval platforms in the U.S. Navy.

Figure 3. Conventional Hull (DDG-51 Arleigh Burke Destroyer). Source: [9].

Operating in harsh Arctic conditions presents a series of obstacles for the Navy. Ship hulls must be reinforced to traverse through the ice. Superstructures must withstand the extreme fluctuating temperatures; pilots must navigate through ice formations. The lack of logistical support and infrastructure to service ships in the region also makes it difficult to operate in this environment [10]. Figure 4 is an image of U.S. Coast Guard ice cutter approaching a stranded tanker ship.

Figure 4. Challenges of Operating in the Arctic. Source: [10].

While ships have already traversed through Arctic waters, research must determine which type of ship hulls is the most efficient in ice conditions. Figure 5 illustrates a swept tumblehome hull and Figure 6 illustrates a wall-sided hull [11].

Figure 5. Tumblehome Hull (DDG-1000 Zumwalt Destroyer). Source: [12].

Figure 6. Wall-Sided Hull (Rossiya, Russian Icebreaker). Source: [13].

The tumblehome hull shown in Figure 5 has sides that are angled inward. The wall-sided hull is more vertical as opposed to being angled. The maritime industry has and continues to explore various types of hull shapes, such as the tumblehome and wall-sided hull, to determine which style has optimal operating conditions in Arctic conditions.

4. Composite Materials

Since the 1940s, the Navy has used composite materials such as fiberglass for small boats and submarine bow domes. However, the Navy has been hesitant to invest in expensive composite materials for the hull structure because there is more risk with these modern materials [14]. While the initial investment for composite ships is significantly higher compared to conventional steel, the high upfront cost is expected to save the Navy money due to reduced maintenance and repair costs [14]. Additionally, composites are typically less noisy and provide increased stealth capability. Figure 7 is an image of the M80 Stiletto, the U.S. Navy's composite-hull prototype ship.

Figure 7. M80 Stiletto. Source: [15].

The M80 Stiletto was built in 2006, and the hull is made from carbon-fiber composite, which is light yet stiff [15]. The M80 Stiletto is a prototype for the next-generation of littoral vessels.

5. Prior Research

Even though significant research has addressed steel-hulled ships operating in Arctic conditions, limited findings cover composite-hulled ships operating in this region. Ships and offshore structures typically experience corrosion, fatigue cracking and localized denting [16]. Within the aviation industry, which uses composite materials, low velocity impacts cause visual damage, but high velocity impacts result in structural penetration, making it a major concern [17]. This research on aviation composites relates to the maritime industry because ships that collide with objects, such as icebergs, are prone to experiencing cracking, delamination, and fiber fracture [17]. NASA also supports the findings on composite materials, stating that cracking and delamination are the most significant on the opposite side of the impact point [18]. Therefore, the integrity of the composite-hull may easily be compromised when traveling through the Arctic region as it collides with ice.

Experimental research has been conducted to determine material properties of non-ice hull ships to determine longitudinal strength and the material yield strength from decreasing temperatures, but limited research has been done on ice loads, which may damage the hull structure, particularly when operating at high speeds [16]. Past studies

using numerical simulations indicated that many times, ship radar systems are unable to detect icebergs less 2 meters in height above the water surface and icebergs that are submerged [19]. Therefore, the ship systems may be unlikely to detect icebergs as the vessel travels through the Arctic. Collision, in both high and low velocity collisions, will make ships prone to plastic deformations, and possibly rupture the hull structure, in cold Arctic waters [19].

A study published in 2010 analyzed the ship colliding with stationary ice. Many studies found the crushing energy of ice to be equal to the available kinetic energy for rigid body ship models [20]. This study used the finite element approach to determine the local plastic deformation on a ship or offshore structure striking ice. The findings revealed that if a structure reacts elastically, the structural deformation is minimal and the work on the structure is negligible. However, when the structure reaches its plastic capacity, the local deformation grows significantly, causing the structure to absorb a significant amount of the energy [20]. Therefore, operating at low speeds minimizes the energy transfer during collisions, resulting in the preservation of the ship's integrity.

Research conducted at the NPS has evaluated different composite-hull shapes that operate in the Arctic region. The different ship hulls were towed at various speeds to determine the force on the ship structure as it collided with ice. The tests revealed that conventional hulls performed the worst in ice conditions while tumblehome hulls had the lowest increase in peak force during impact [11].

Note that the past experiments evaluated ship-like hull models that interacted with floating ice or ice fields. The research identified potential damage to ship hulls operating at high speeds and the type of ship hulls that are most suitable for the Arctic region. However, limited data addresses how ships respond to wave forces while colliding with an ice field.

B. OBJECTIVES

This study specifically evaluated the stress and strain of composite material moving through an ice field. The project goal was to analyze the scenario numerically and to build a wave generating system. This project creates the foundation for future numerical research with the application of wave forces.

1. Numerical Objective

The Dynamic System Mechanics Advanced Simulation (DYSMAS) program evaluated a composite ship moving through an ice field using the finite element approach [21]. A large box was built in to simulate a ship hull that had identical properties to composite e-glass. A smaller box was also constructed to represent sea ice.

Note that DYSMAS is designed to evaluate underwater explosions. Therefore, a major obstacle was to determine whether the program could properly evaluate a ship colliding with ice, as opposed to an explosion. The computational models were completed over the following phases:

Phase 1: A “ship,” represented in this study as a cubic box, was built in DYSMAS with e-glass material properties. It had a prescribed kinematic velocity and collided with ice. The user recorded the stress and strain on the ship for the following parametric studies, listed in Table 1.

Table 1. Parametric Study

Parameter	**Modification**
Ship Speed [m/s]	2.5, 5, 10
Ice Cube Size [cm]	5, 15, 30
Number of Ice Cubes	1, 3, 5

The objective of altering the listed parameters was to determine how the various velocities would affect the bow wake, stress, and strain on the ship hull. The data was analyzed qualitatively through stress fringe diagrams and quantitatively through time history plots.

Phase 2: The second phase was to alter the ship hull shape. By changing the shape of the hull, the fluid flow and bow wake also changed. There were three different hull shapes that were tested:

- Vertical Hull
- Tumblehome Hull
- Flared Hull

The vertical hull was used throughout the simulations in Phase 1. Note that the tumblehome hull and the flared hull were tested at a ship speed of 5 m/s, a hull thickness of 2 mm. Both ship hulls also collided with one 5 cm ice cube.

The computational data can be validated in the NPS tow tank. Note that the experiments in the tow tank are restricted to the dimensions of the channel and the speed of the tow carriage. Therefore, the computational analysis in DYSMAS allows greater flexibility because the ship model can move at realistic speeds, and the area that the ship moves through may be modified. Regardless, the experimental tests are essential in validating the computational results.

2. Experimental Objective

The goal of the experimental tests was to design and build a wave generating system in the NPS tow tank. The purpose of the wave generating system is to allow future research of towing a composite “ship” through the channel as it collides with ice blocks and waves. The three necessary components for these tests are the testing channel, the tow carriage, and a wave maker. The testing channel and tow carriage equipment were already available in NPS tank. However, the tank did not have a wave generator; therefore, a primary objective for this thesis was to construct a wave maker. The experimental objects had the following phases:

Phase 1: The first phase was to design the wave generator. It was important to evaluate the most suitable mechanism for the tank. A criterion was to make minimal alterations to the tank and not to disrupt the tow carriage.

Phase 2: After designing the wave generator, the next procedure was to search for the proper equipment, purchase the necessary materials, and assemble the parts.

Due to the limited time of this year-long thesis, the wave generating system was not calibrated or tested. However, the design and construction provides the opportunity for future experimental research.

THIS PAGE INTENTIONALLY LEFT BLANK

II. METHODOLOGY: NUMERICAL MODELING AND SIMULATION

This thesis used DYSMAS to conduct the numerical simulations of composite-hull ships colliding with ice. Section A of this chapter provide a general overview of how DYSMAS functions from the code architecture to the phases of code execution. Section B provides the user's methodology of conducting the parametric study, such as ship speed, ice cube size, number of ice cubes, and hull shape.

A. CODE OVERVIEW

As stated in the DYSMAS manual, this program is managed by the Department of Defense and developed collaboratively between the U.S. Navy and Lawrence Livermore. The program couples Gemini, the fluids component, with Dyna, the structures component [21]. Gemini was developed and is managed by the Naval Surface Warfare Center Indian Head Division while Dyna is managed by Lawrence Livermore National Laboratory. Figure 8 illustrates that DYSMAS combines shock and fluid dynamics with structural response and damage, making it a powerful program.

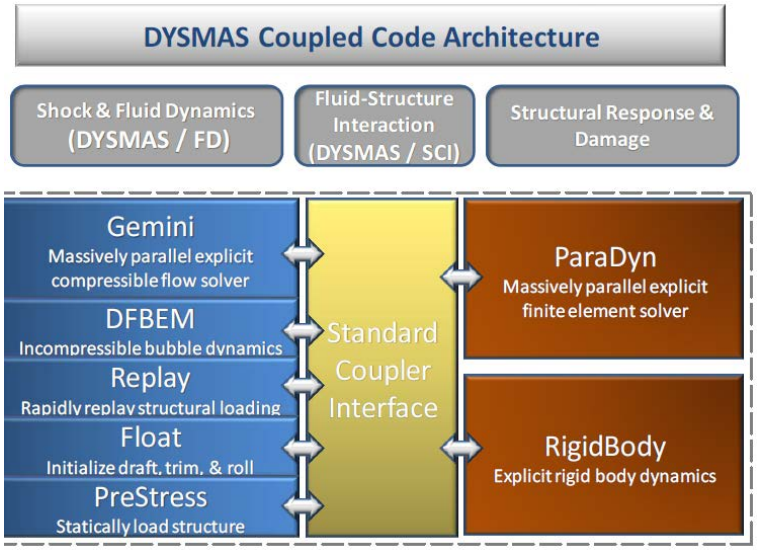

Figure 8. DYSMAS Code Architecture. Source: [21].

As previously stated, DYSMAS' two main components are Gemini and Dyna. The Gemini component is a fluid code that uses the Eulerian specification to analyze the fluid flow field. The Dyna component uses the Lagrangian specification to analyze the structure. The program analyzes fluid motion of individual fluid particles that are observed through space and time.

1. Gemini and Dyna Code

The Gemini uses the Godunov method to analyze the Euler fluid mesh at various time steps. Note that the program examines the Euler cell through a one-dimensional approach, and the code assumes inviscid flow [22].

The Dyna code uses a three-dimensional finite element approach to analyze the dynamic structural response. Note that the structure may be built directly in the DYSMAS' preprocessing program or in external programs, such as Solidworks and Rhino. The user built the structures directly in DYSMAS for this thesis. Figure 9 is a chart that illustrates the program data flow.

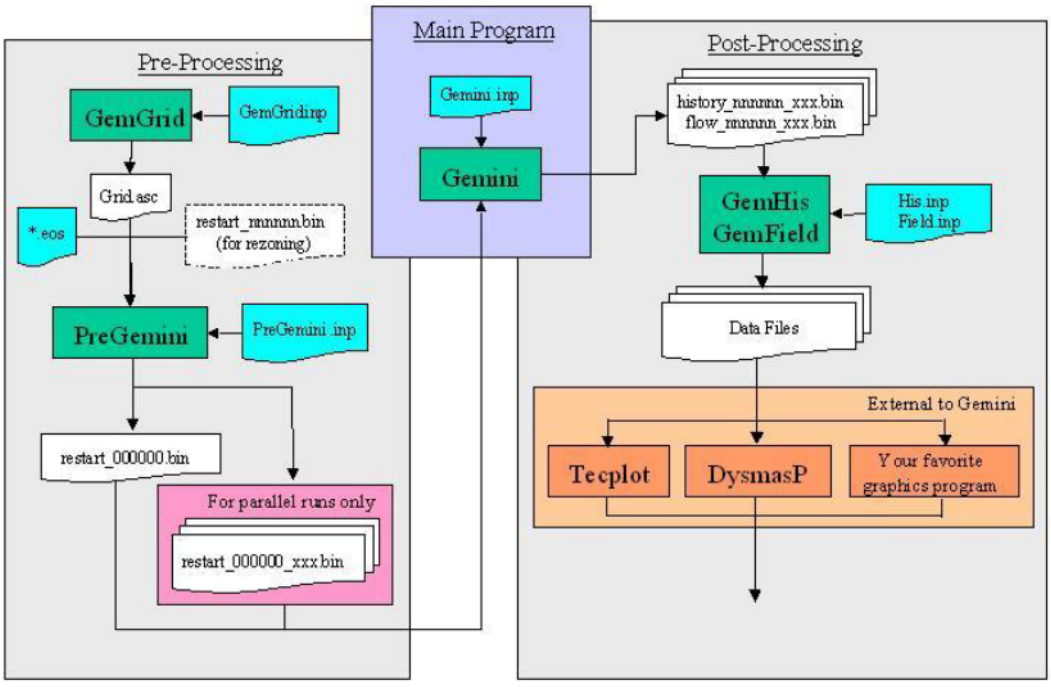

Figure 9. DYSMAS Data Flow. Source: [21].

Figure 9 shows that the Gemini code is divided into three stages: pre-processing, main program, and post-processing. In the pre-processing stage, the PreGemini code is executed, which consists of building the structure and running the grid. The user builds the fluid grid by specifying the size in the X, Y, and Z coordinates. The user also constructs the structure and positions it into fluid. Lastly, this stage requires the assignment of material properties for the fluid and structure.

The main program uses the Gemini code to runs the transient analysis between the fluid and structure. The program uses a finite-difference solver and runs on the Hamming high computer cluster. DYSMAS analyzes the force and pressure on both the fluid and structure domains. Rather than providing a general solution, DYSMAS determines the fluid and structural response at each time step.

The post-processing stage allows the user to build contour plots and graphs. The files produced from the main Gemini code are processed to generate fringe animations and two-dimensional graphs. Additionally, the program provides nodal and elemental data, such as displacement, velocity, acceleration, stress, and strain. The following section provides an overview of how DYSMAS couples Gemini with Dyna.

2. Standard Coupler Interface

The standard coupling interface (SCI) links together the Gemini and Dyna components. The SCI couples the Euler fluid with the structure's nodes and elements. Figure 10 is a block diagram depicting the information passed the Gemini and Dyna through the SCI.

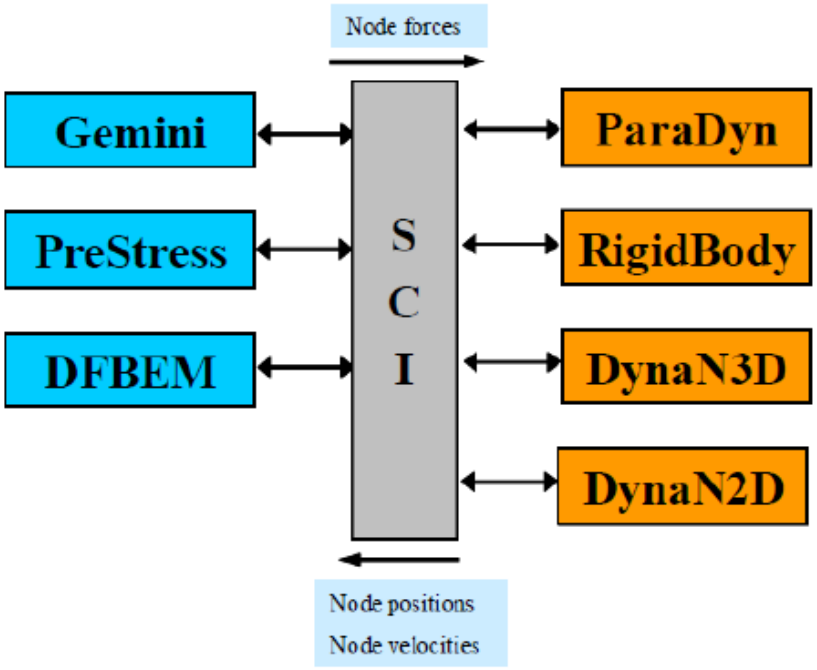

Figure 10. Standard Coupling Interface. Source: [22].

In Figure 10, the blue boxes on the left represent Gemini fluid component while the orange boxes on the right represent the structural component. By merging these parts, DYSMAS analyzes the transient response of the components simultaneously. The following section provides an overview of how to execute the DYSMAS program. The following section provides an overview of the user's methodology to complete the thesis' parametric study.

B. PARAMETRIC STUDY

In this thesis, the user conducted multiple simulations to refine the appropriate properties for the parametric study. Section 1 describes the fluid grid, material properties, and boundary conditions. Section 2 provides an overview of how the structure and ice were built in DYSMAS. Section 3 through 6 explain the various stages of the parametric study, which consisted of manipulating the ship speed, ice cube size, number of ice cubes, and hull shape.

1. Gemini Euler Field

The user built the Euler fluid grid in the pre-processing step, specifying the number of cells, cell width, material properties, and boundary conditions. Table 2 summarizes the fluid grid used for the data runs.

Table 2. Fluid Grid Parameters

	Material	**Number of Cells**	**Coordinate Width [cm]**	**Boundary Condition 1**	**Boundary Condition 2**
X Coordinate	Tillotson Water	33	100	Wall	Wall
Y Coordinate	Tillotson Water	83	251	Wall	Free
Z Coordinate	Tillotson Water	33	100	Wall	Water-Air
	Air	12	40	Water-Air	Free

Table 2 lists the fluid grid parameters. The two fluid materials used in this thesis were water and air. The fluid mesh is quadrilateral and the user defined the mesh size by specifying the number of cells within the coordinate width. The wall boundary replicates the wall conditions of a tow tank, causing wave reflection to occur. The free boundary condition in the Y coordinate represents a long tank channel; therefore, wave reflection is nonexistent. The Z coordinate consists of two layers. The top layer is air and below is the water layer. The equations of state for the air and water are listed in Appendix A.

The fluid field from the parameters listed in Table 2 is illustrated in Figure 11.

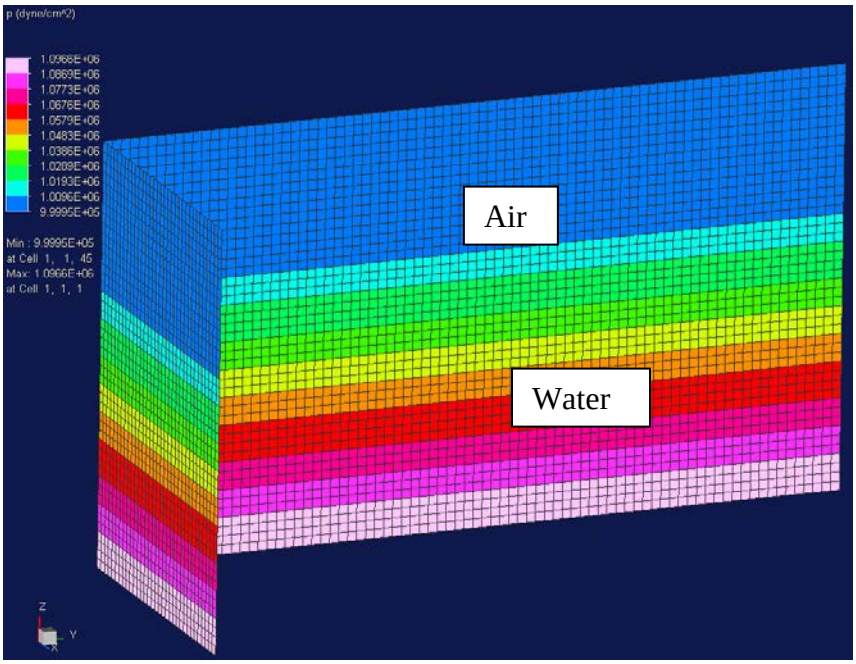

Figure 11. Fluid Field

The dark blue upper layer illustrates the air and the color fringe below represents the water. The water column changes due to the hydrostatic pressure, which increases with depth. After generating the fluid grid, the next step is to build the structure.

2. Dyna Lagrangian Structure

The user constructed the ship and ice blocks in DYSMAS' pre-processing stage. The ship was a 30 cm cube with e-glass material properties, and the ice was a 5 cm cube. The material properties for e-glass and ice are listed in Table 3.

Table 3. Dyna Structure Material Properties. Source: [23].

	Element Type	Density (kg/ m^3)	Poisson Ratio	Modulus of Elasticity [MPa]
E-glass	Elastic Shell	2000	0.15	18000
Ice	Rigid Solid	913	0.33	9.00

Figure 12 depicts the purple ship, orange ice block, and light blue still water level plane. The ship is neutrally buoyant and the ice block is submerged 90%, which is typical for sea ice. Note that the coordinate frame, as shown in Figure 12, is consistent for the rest of the figures.

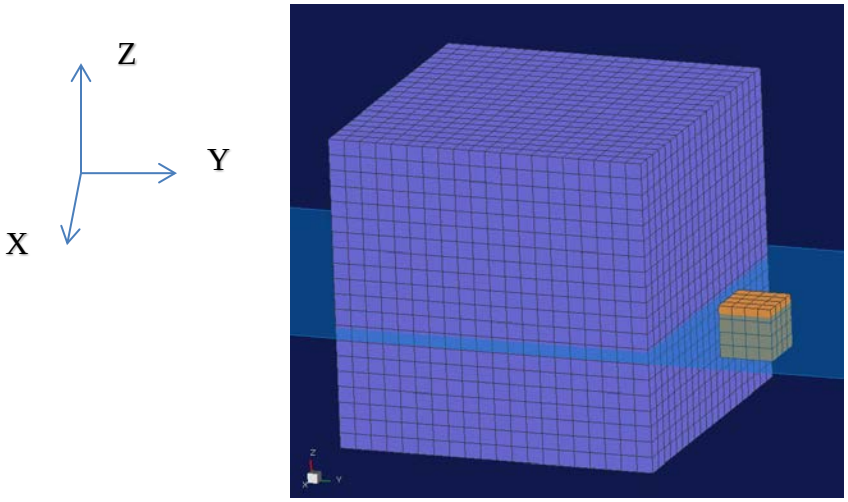

Figure 12. Ship and Ice Block

In Figure 12, the ship is the large purple cube while the ice block is the smaller orange cube. The ship was a 30 cm shell cube with a Hughes-Liu shell element formulation. The structure was built as a single quadrilateral shell with a thickness of 0.002 m. The ship's mesh was 1.5 cm by 1.5 cm. The ice cube was placed 2 cm away from the ship and built as a rigid body with a mesh size of 1.25 cm by 1.25 cm. The user submerged the ice by 90%, which is typical for floating sea ice.

A sliding with friction interface was set between the ship and ice block. The ship was the "master" and the ice block was the "slave" for the sliding interface. Only the front side of the ship hull that hits the ice block had a set sliding interface, but the entire ice cube had a prescribed sliding interface. Additionally, the user constrained the top layer of nodes on the ship in the X and Z axis. This constraint is representative of the Naval Postgraduate's tow tank. Note that the tank's system connects towed object at the top and only allows movement down the tank channel, or Y axis. Thus, the top nodes of the ship freely moved in just the Y axis, shown in Figure 13.

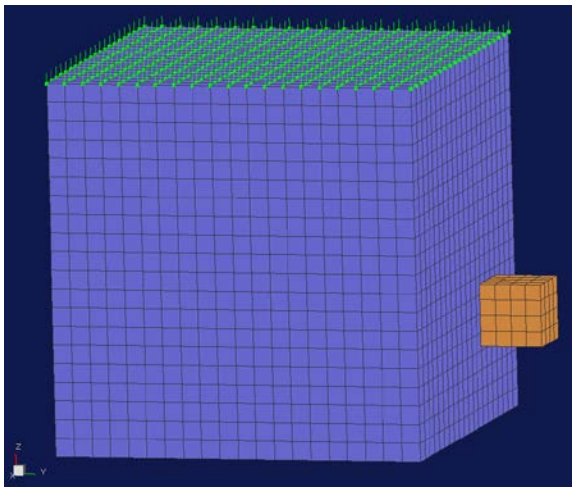

Figure 13. Nodal Constraints in the X and Z Coordinates

The user determined the effective stress, x-axis strain, and y-axis strain by assigning element time histories. Due to high computation time, the user selected certain elements, as shown by the green boxes, instead of the entire ship, shown in Figure 14.

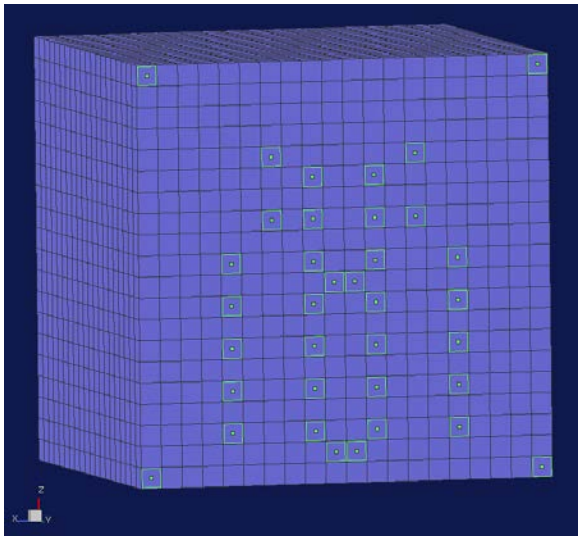

Figure 14. Selected Time History Elements

The time history analysis generates stress and strain curves in the post-processing procedure. Since the ship is built from composite e-glass, there are multiple layers in the shell element. Compared to the inner layers, the outer layer experiences the greatest

amount of stress and strain. Therefore, the outer layer was selected as the integration point for the time history analysis.

For the velocity study, the time history plots were not used to determine the effective stress. Instead, the researcher used the color fringe animation to determine the effective stress. The researcher used the color fringe because of the high structural deformation during the velocity tests, which will be further discussed in Chapter III.

The final step was to define the coupling interface between the Dyna structures with the fluid grid. The following sections provide an overview of the changes for the parametric study.

3. Ship Speed

The overall goal of the ship speed parametric study was to determine whether there are trends between increased ship velocities with stress and strain. The ship speed increased from 2.5 m/s to 5, 7.5, and 10 m/s. Figure 15 illustrates the prescribed kinematic velocity applied to the top layer of nodes on the ship.

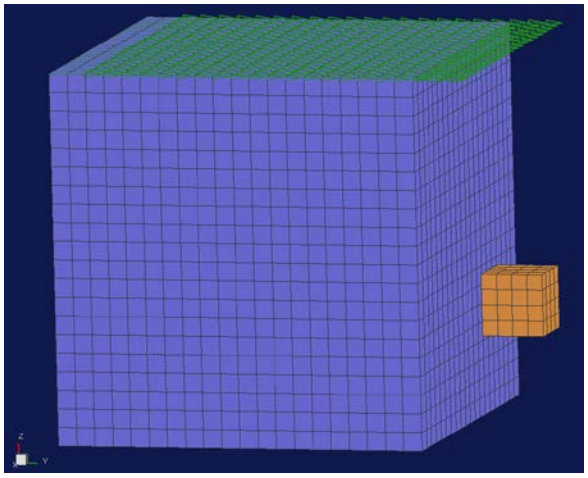

Figure 15. Prescribed Kinematic Velocity on Ship Nodes

Only the top nodes of the ship had prescribed kinematics in order to replicate the towing mechanism in the Naval Postgraduate tow tank. The ice block was stationary with

no applied loads, forces, or kinematics. This allowed the ice to move freely and collide with the ship hull.

4. Ice Cube Size

The second parametric study was to analyze the stress and strain on the ship by increasing the ice cube size. The 5 cm ice block was used for the initial tests. Next, the 15 cm ice cube, which is half the ship size, and 30 cm, which is equivalent in size to the ship, were used. Figure 16, Figure 17, and Figure 18 illustrate the tests conducted for this parametric study.

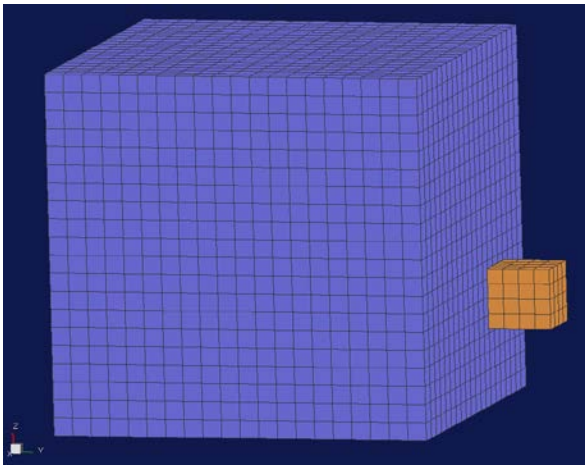

Figure 16. 5 cm Ice Cube Block

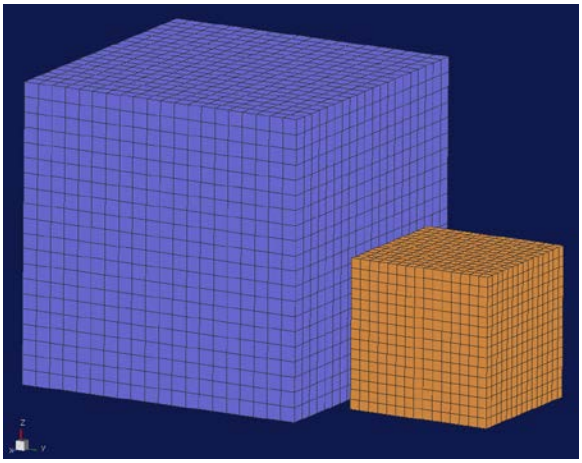

Figure 17. 10 cm Ice Cube

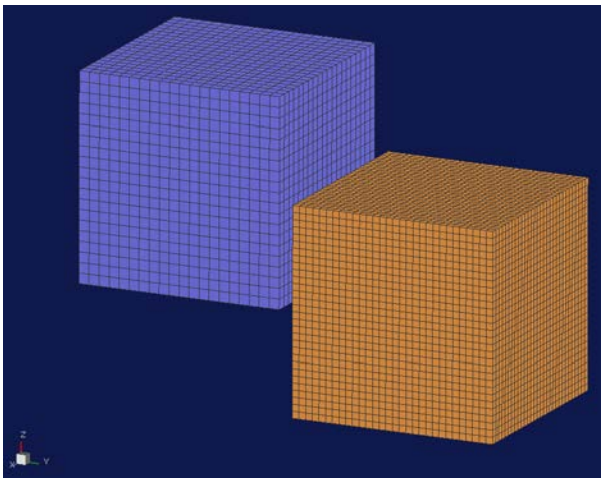

Figure 18. 30 cm Ice Cube

Note that all of these tests were conducted with a ship velocity of 5 m/s. After these tests were completed, the stress and strain on the ship hull was analyzed.

5. Number of Ice Cubes

Another parametric study was to analyze the effects of increasing the number of ice cube blocks in the fluid field. This original study used one 5 cm ice cube block. Therefore, a total of three and five 5 cm ice cube blocks were added. The coordinate system for the ice cubes are listed in Table 4.

Table 4. Location of Ice Blocks

Test	Ice Block Number	X [cm]	Y [cm]	Z [cm]
1 Block	1	12.5	32	7.5
3 Blocks	1	2.5	32	7.5
	2	12.5	32	7.5
	3	22.5	32	7.5
5 Blocks	1	2.5	32	7.5
	2	12.5	32	7.5
	3	22.5	32	7.5
	4	7.5	40	7.5
	5	17.5	40	7.5

Images of the three and five ice cubes parametric study are shown in Figure 19 and Figure 20, respectively. Note that a 5 m/s ship speed was used for these tests.

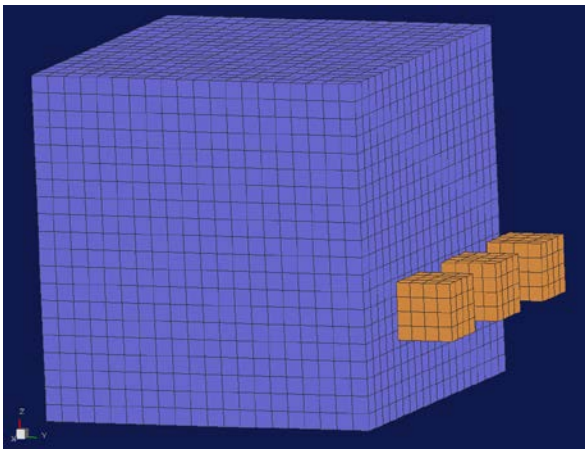

Figure 19. Three Ice Cube Blocks

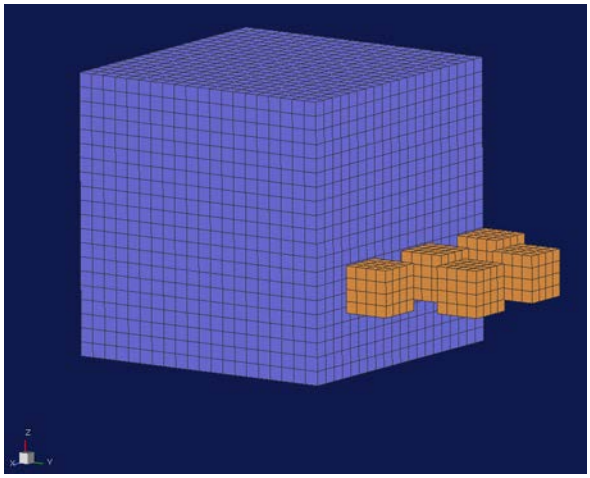

Figure 20. Five Ice Cube Blocks

6. Hull Shapes

The last parametric study analyzed different hull shapes. All of the previous tests utilized a vertical hull; therefore, this study examined tumblehome and flared hulls. For these tests, the ship speed was also constant at 5 m/s and the ship collided with one 5 cm ice block. Figure 21 illustrates the tumblehome hull and Figure 22 illustrates a flared hull. Both hulls had a slope of ~30 degrees from the z-axis. The elements used for the time history analysis are shown in Figure 23 and Figure 24.

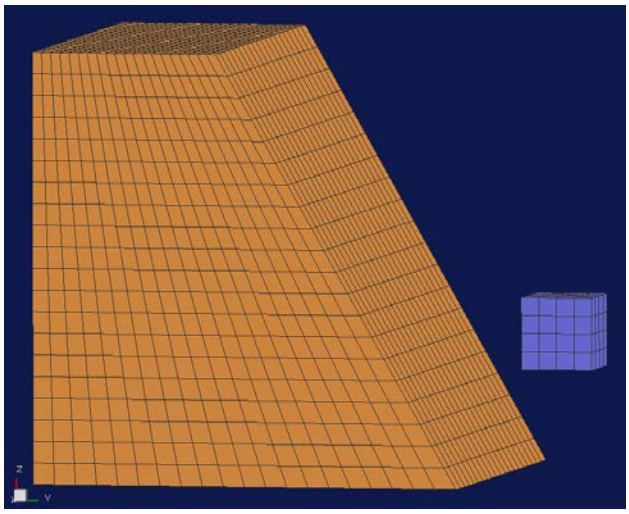

Figure 21. Tumblehome Hull

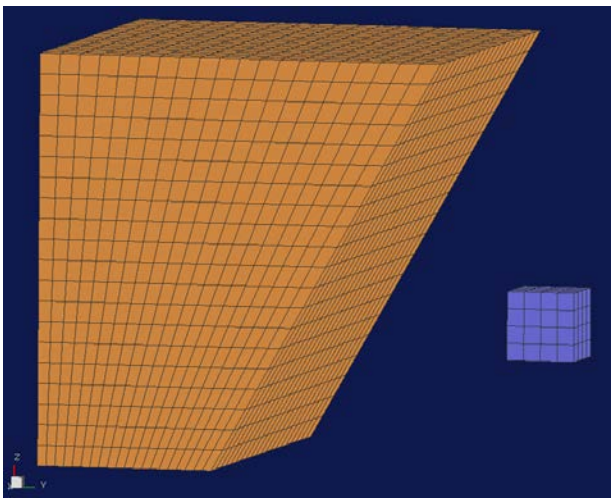

Figure 22. Flared Hull

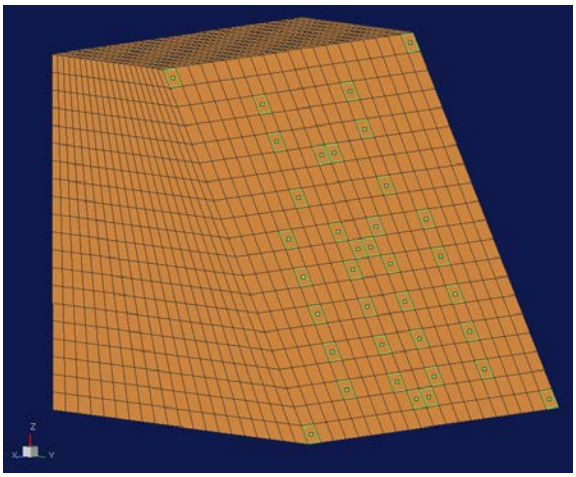

Figure 23. Time History Elements for Tumblehome Hull

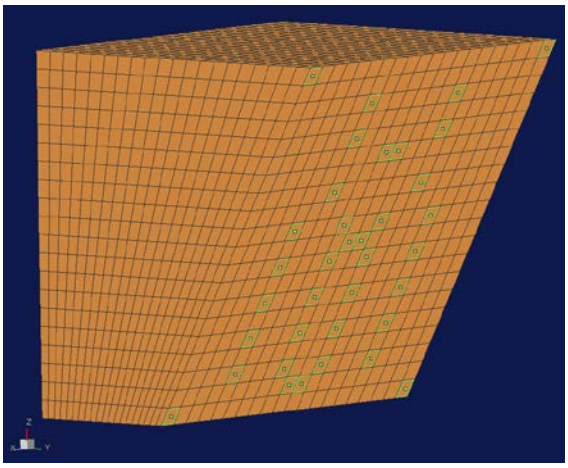

Figure 24. Time History Elements for Flared Hull

The overall purpose of the parametric study was to determine how the various conditions affected the stress and strain on the ship. This section provided an overview of the DYSMAS code and the conditions used for the numerical simulations. The chapter also provides an overview of the alterations conducted on the ship speed, ice cube size, number of ice cube, and hull shape for the parametric study of the thesis.

In addition to the numerical simulations, a second portion of the thesis was experimental modeling. The NPS has a tow tank, but no wave generation capability. Therefore, the goal was to build a wave generator that would be used for future experimental modeling.

III. NUMERICAL RESULTS AND DISCUSSION

DYSMAS computed the results of a ship colliding with ice. The simulations examined the effects of increasing ship velocity, ice cube size, number of ice cubes, and hull shape on a composite ship.

Note that for all of the runs, the data analyzed fell between 0.01 sec and 0.2 sec. The ship accelerating to its prescribed kinematic velocity caused the spikes in the time history plots. Since this study analyzed the stress and strain when the ship begins to collide with the ice and not when the ship accelerates to its prescribed velocity, time intervals less than 0.01 sec have been excluded. Figure 25 shows excessive initial spikes caused during the numerical simulations.

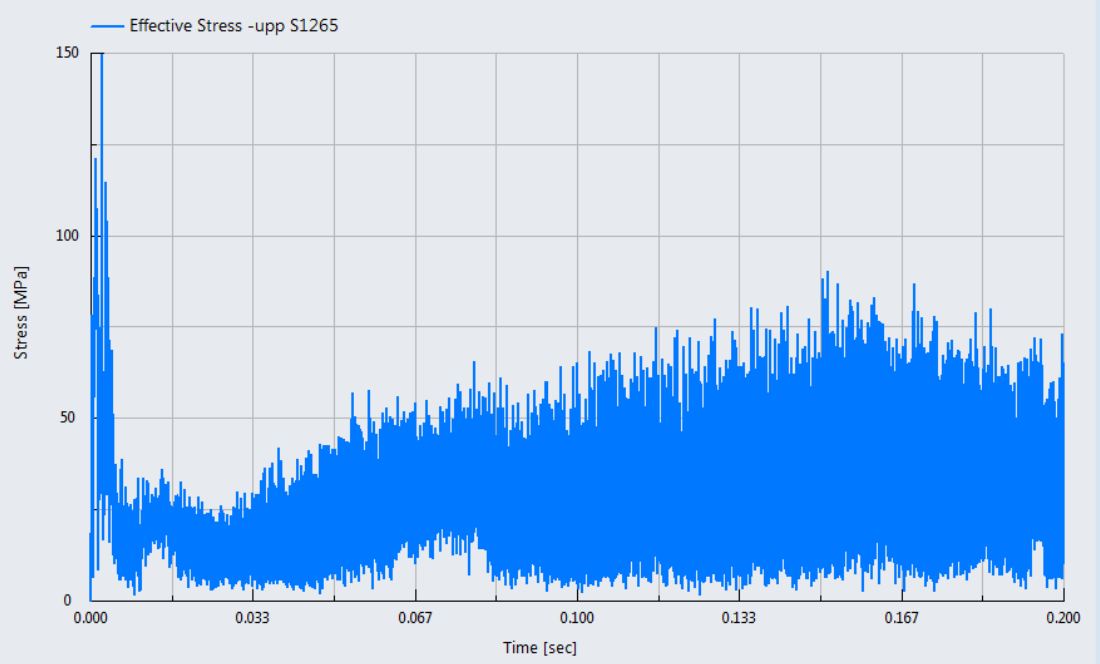

Figure 25. Time History Plot

The various tests determined the maximum effective stress, the X-strain, and the Z-strain, but not the Y-strain since the ship moved in the Y-direction. It was too computationally expensive to analyze the entire face of the ship hull; therefore, the

researcher selected specific elements shown in Figure 14 for vertical hulled ships, Figure 23 for tumblehome hulls, and Figure 24 for flared hulls. The selected elements were dispersed throughout the hull face, but note that the quantitative data could be improved by selecting additional elements. The following sections provide the results and discussion on the parametric study.

A. ALTERING SHIP VELOCITY

This study analyzed how varying the ship speed affects the stress and strain on the hull. The 5 cm stationary ice block was kept constant throughout the ship speed tests of 2.5, 5, 7.5, and 10 m/s. As mentioned in Chapter II, the color fringe animation measured the effective stress. In order to establish a baseline, the user conducted the velocity tests with and without the ice blocks. This test analyzed the front face of the ship, which is the side that collides with the ice. The results for the test are shown in Figure 26.

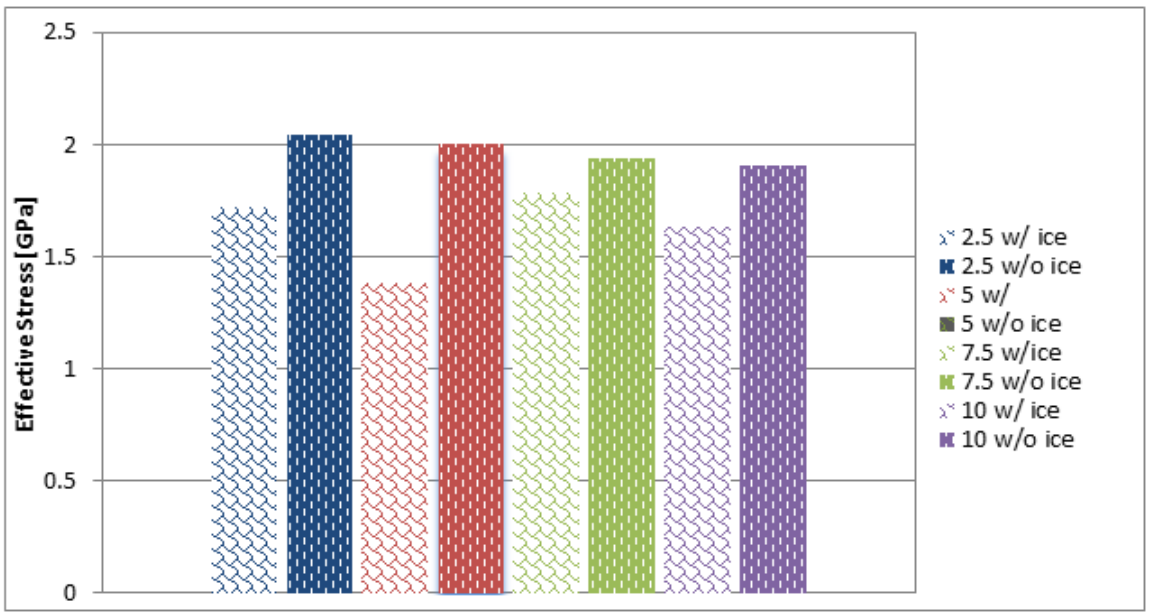

Figure 26. Effective Stress for Velocity Test on Front Face of Ship

Figure 26 reveals that there is no clear trend between the effective stresses on the front face of the ship with increasing velocity. The researcher qualitatively examined the location of maximum effective stress on the ship's front face and noticed that the location

changed throughout the simulations. Figure 27 through Figure 30 illustrate the location of effective stress on the ship at various time steps.

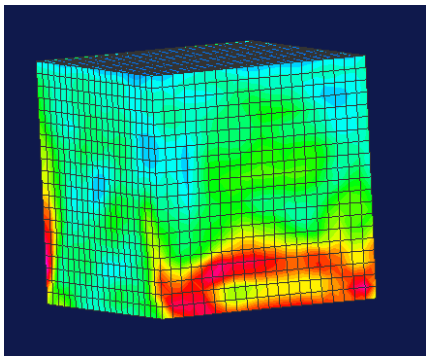

Figure 27. Effective Stress at 0.01 sec

Figure 27 shows the stress acting on the ship at 0.01 sec. The ship experiences a high degree of stress at the bottom of the front face, which is the side that collides with the ice block. As the simulation continues, the ship's front face no longer experiences a high level of stress, as shown in Figure 28.

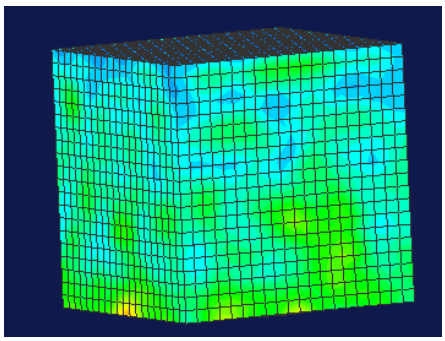

Figure 28. Effective Stress at 0.1 sec

The high concentration of effective stress continues to change throughout the simulation. At 0.15 sec, the effective stress begins to move toward the front of the ship, as depicted in Figure 29. The high effective stress returns to the front face when the simulation ends at 0.2 sec, as shown in Figure 30.

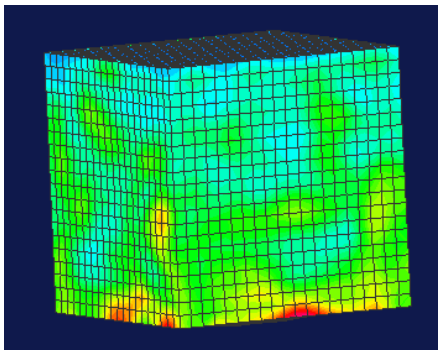

Figure 29. Effective Stress at 0.15 sec

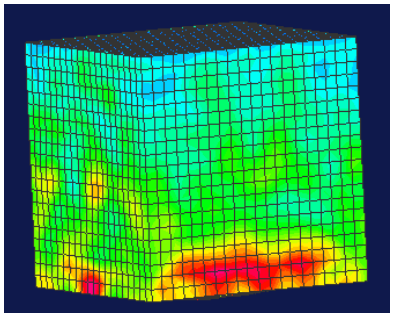

Figure 30. Effective Stress at 0.2 sec

The purpose of Figure 27 through Figure 30 was to qualitatively show that the effective stress locations for the velocity tests are not fixed. This change in location occurs because the ship was built as a very thin elastic shell. The ship is constantly flexing due to the fluid flow and ice block collision. The high speed causes the elastic shell to bend as the ship undergoes compression. Therefore, the researcher next analyzed the maximum effective stress on the entire ship hull instead of just the front face. The researcher also determined the maximum effective stress by using the color fringe. Figure 31 shows the results of the test.

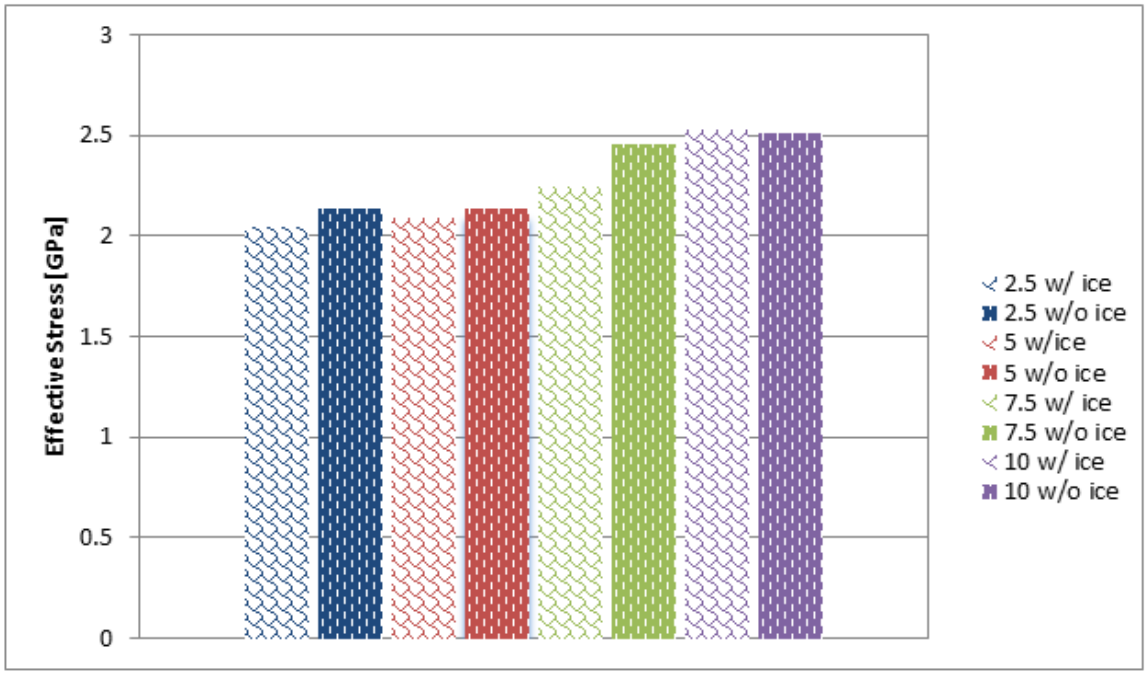

Figure 31. Effective Stresses of Velocity Tests for Entire Ship Hull

The purpose of running the simulation with and without ice was to determine the impact of the ice blocks. The user expected the ice blocks to increase the maximum effective stress on the ship. However, the data revealed that the simulations without the ice block actually had a higher effective stress, except for the 10 m/s test. The simulation with and without ice for the 10 m/s block had similar effective stresses because the bow wake pushed away the ice cube early in the simulation. Therefore, only the fluid dynamics caused the effective stress which explains their similarity.

When the ice block collides with the ship, it provides pressure against the ship hull. The ship was built as a thin elastic shell and easily bends from the fluid flow. The ice essentially provides resistive loading for the ship hull, which helps explain why the simulations without ice had higher effective stresses. Figure 32 illustrates the ice acting as a resistive load compared to a simulation without ice.

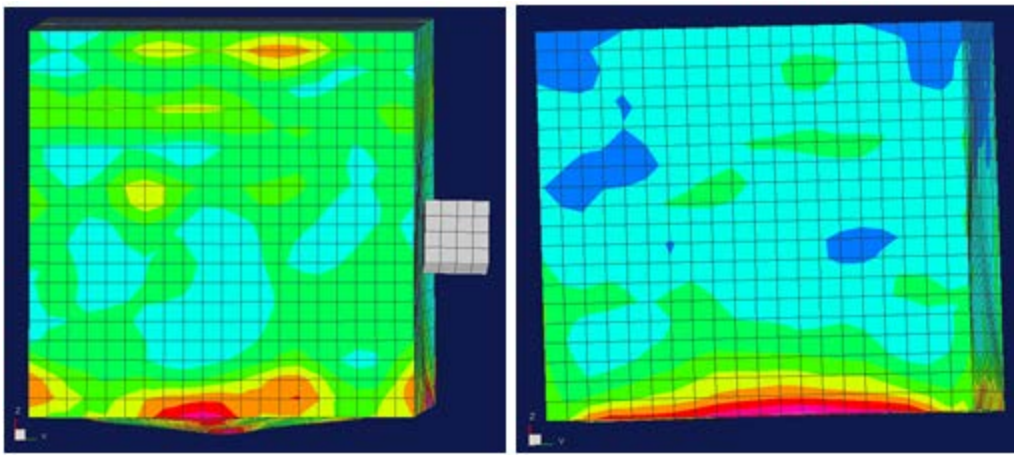

Figure 32. Ice Providing Resistive Loading

Additionally, the user expected that higher ship velocities result in higher effective stress on the ship, which is confirmed by Figure 31. However, even though the 2.5 m/s ship is one third the speed of the 7.5 m/s ship, its effective stress is only slightly lower. Therefore, the researcher examined the ice cube position to determine whether the position changed the maximum effective stress. Figure 33 through Figure 36 provide illustrations of the numerical simulation at various velocities.

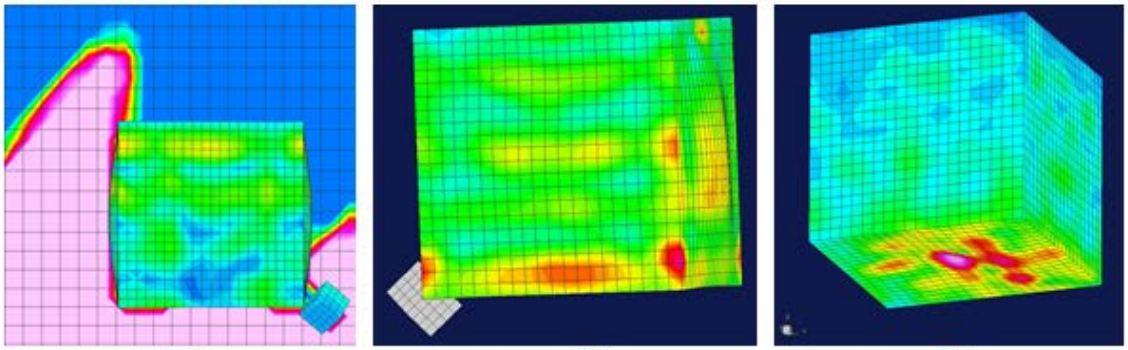

Figure 33. Graphic for 2.5 m/s Velocity Test GPa.

In Figure 33, the data is shown at 185 msec. (a) For the structure, the minimum velocity is 0.26 m/s and the maximum velocity is 2.77.6 m/s. The minimum fluid density is 0.00 g/cm^3 and the maximum density is 1.0 g/cm^3. (b) The effective stress on the ship is

shown. The minimum value was 13.212 MPa and maximum value was 2.039 GPa. (c) This figure was for the simulation without ice. The minimum effective stress was 22.163 MPa and the maximum was 2.1276

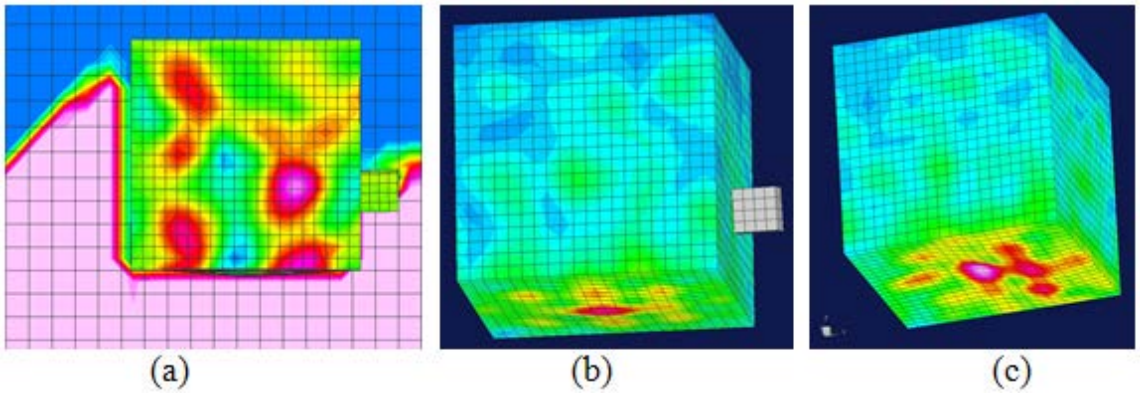

Figure 34. Graphic for 5 m/s Velocity Test

In Figure 34, the data is shown at 199 msec. (a) For the structure, the minimum velocity is 0.473 m/s and the maximum velocity is 11.9 m/s. For the fluid, density is shown. The minimum density is 0.00 g/cm^3 and the maximum density is 1.0 g/cm^3. (b) The effective stress on the ship is shown. The minimum value was 10.328 MPa and maximum value was 2.089 GPa. (c) This figure was for the simulation without ice. The minimum effective stress was 22.163 MPa and the maximum was 2.1276 GPa.

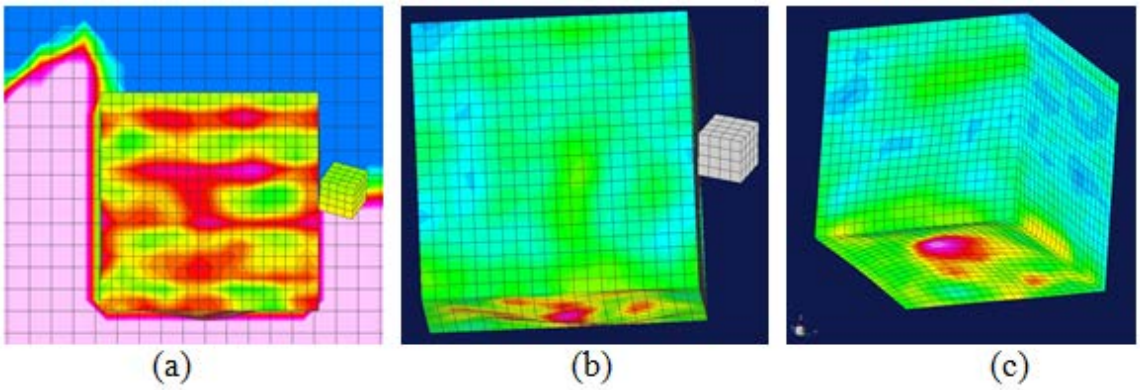

Figure 35. Graphic for 7.5 m/s Velocity Test

In Figure 35, the data is shown at 173 msec. (a) For the structure, the minimum velocity is 0.483 m/s and the maximum velocity is 21.6 m/s. For the fluid, density is shown. The minimum density is 0.00 g/cm^3 and the maximum density is 1.0 g/cm^3. (b) The effective stress on the ship is shown. The minimum value was 39.392 MPa and maximum value was 2.245 GPa. (c) This figure was for the simulation without ice. The minimum effective stress was 24.526 MPa and the maximum was 2.45269 GPa.

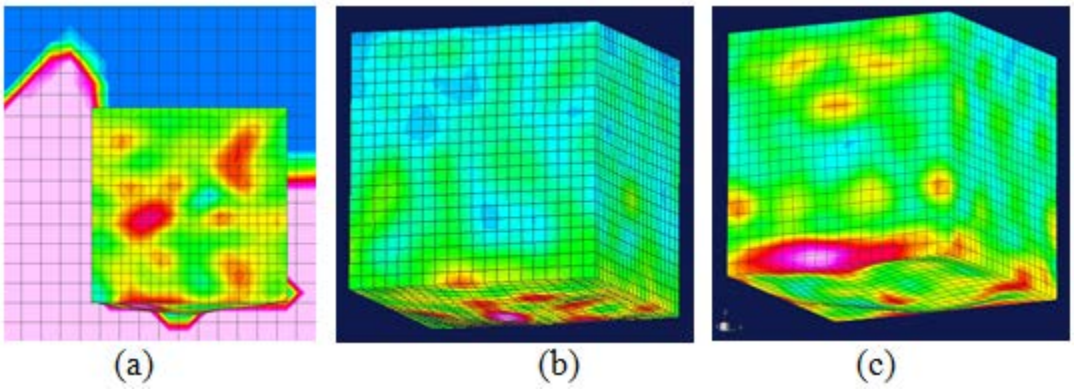

Figure 36. Graphic for 10 m/s Velocity Test

In Figure 36, the data is shown at 148 msec. (a) For the structure, the minimum velocity is 0.224 m/s and the maximum velocity is 24.7 m/s. For the fluid, density is shown. The minimum density is 0.00 g/cm^3 and the maximum density is 1.0 g/cm^3. (b) The effective stress on the ship is shown. The minimum value was 27.045 MPa and maximum value was 2.528 GPa. (c) This figure was for the simulation without ice. The minimum effective stress was 122.45 MPa and the maximum was 2.546 GPa.

Figure 33 shows that in the 2.5 m/s test, the edge of the ice block hits the corner of the ship hull. The ice block in the 5 m/s simulation is flush against the hull. The load from the ice block is thus distributed over multiple elements. In contrast, when the ice cube corner strikes the ship, it acts as a stress concentrator, resulting in a high effective stress.

The ice block's entire edge collides with the ship in the 7.5 m/s scenario. Therefore, the load is still distributed over several elements, but not as many elements as

the 5 m/s scenario. The position of the ice blocks help explain why the maximum effective stresses on the ship are fairly close for the 2.5, 5 and 7.5 m/s scenarios despite the drastic difference in ship speed.

The data reveals that the fluid flow and ice block position had a major effect on the effective stress. When the corner of the ice block collides with the ship, the corner acts as a stress concentrator, yielding the highest effective stress. However, when the edge of the block collides with the ship, the force from the cube is distributed over multiple elements, and thus, the effective stress is lower. It can be concluded that ship speed affects the effective stress, but the ice cube position has a higher contribution to the maximum stress.

B. CHANGING ICE CUBE SIZE

The next parametric study tested various ice cube sizes to determine whether larger ice cubes affected the effective stress and strain on the ship hull. The cubes were increased from 5 cm, to 15 cm, and then to 30 cm. The 15 cm ice block was half the size of the ship and the 30 cm ice block was equivalent in size to the ship. For these tests, the ship maintained a constant 5 m/s velocity and the ice block was submerged by 90%. Figure 37 illustrates the effective stress results from the numerical simulations.

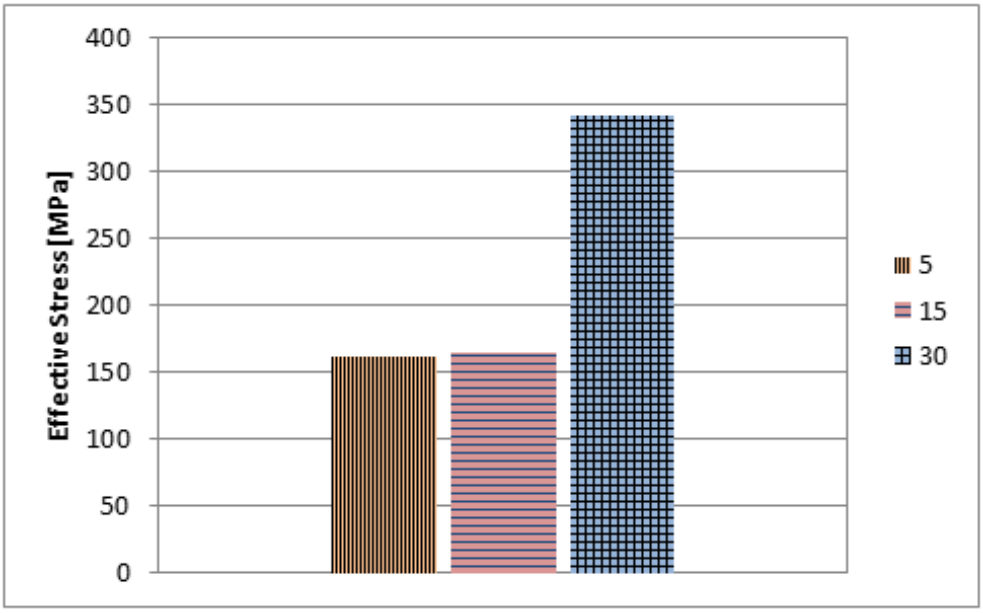

Figure 37. Effective Stresses for Ice Block Size Tests

As expected, the larger ice cubes result in higher effective stress on the ship hull. The ship had to “push” the 30 cm ice block because they were equivalent in size, shown in Figure 38.

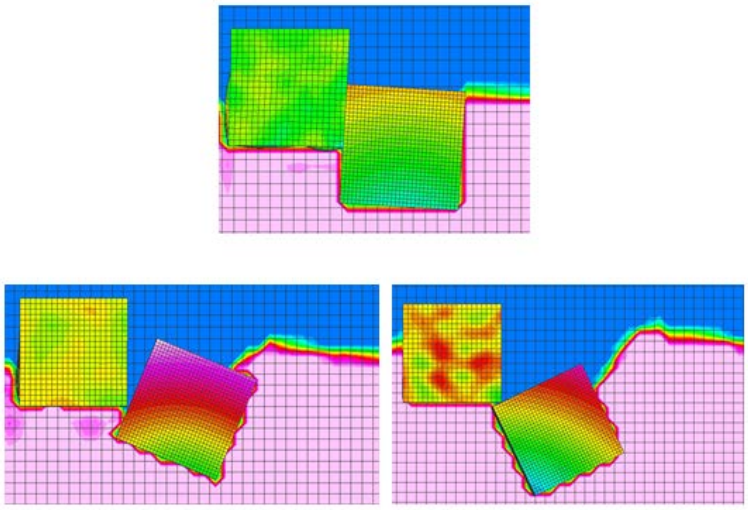

Figure 38. Graphic for 30 cm Ice Cube

In Figure 38, the maximum effective stress is found at 31.5 msec. For the structure, the minimum velocity is 0.322 m/s and the maximum velocity is 15.7 m/s. For the fluid, density is shown. The minimum density is 0.00 g/cm^3 and the maximum density is 1.0 g/ cm^3. Since the 30 cm ice block is submerged by 90%, the block is pushed until it rotates under the ship. As a result, an extremely large wake is formed.

Figure 39 shows that instead of being pushed and rotated underneath the ship like the 30 cm block, the 15 cm ice block rides the with the bow wake after initally collison.

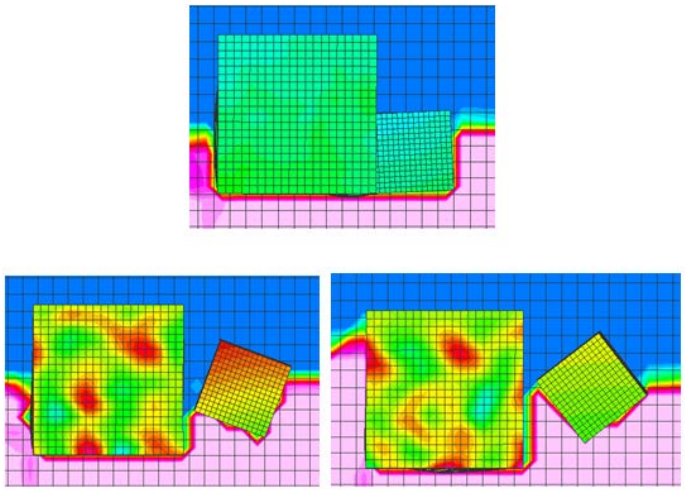

Figure 39. Graphic for 15 cm Ice Cube

In Figure 39, the maximum effective stress is found at 189.9 msec. For the structure, the minimum velocity is 0.257 m/s and the maximum velocity is 21.6 m/s. For the fluid, density is shown. The minimum density is 0.00 g/cm3 and the maximum density is 1.0 g/ cm^3.

The user did not expect the 5 cm ice block to have a maximum effective stress almost equivalent to that of the 15 cm block, graphed in Figure 37. While the 15 cm ice block rides the bow wake during the simulation, the 5 cm ice block is trapped in front of the ship and thus, continuously collides with the hulll, shown in Figure 40.

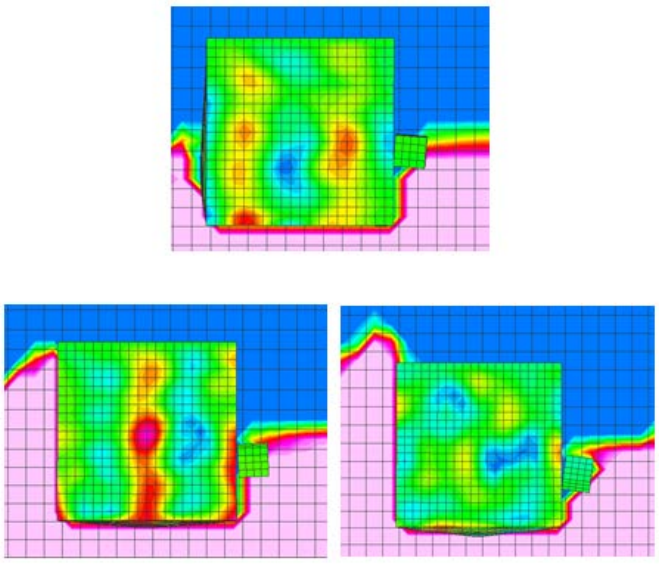

Figure 40. Graphic for 5 cm Ice Cube

In Figure 40, the maximum effective stress is found at 199 msec. For the structure, the minimum velocity is 0.561 m/s and the maximum velocity is 18.3 m/s. For the fluid, density is shown. The minimum density is 0.00 g/cm^3 and the maximum density is 1.0 g/cm^3.

From these tests, it may be concluded that the position at which the ice block collides with the ship has the greatest impact on the effective stress. The 5 cm ice block is significantly smaller than the 15 cm ice block, yet the maximum effective stresses between the two tests were almost equivalent. The 30 cm ice cube was an extreme scenario, but it still followed the same trend. Both the structure and ice cube remained intact because the ship is an elastic shell and ice is a rigid body. In a physical application, the ship or ice would split from the high speed collision. The results from the velocity test indicated that the ice cube location impacted the effective stress on the ship, and this ice cube size study reconfirmed that hypothesis.

Note that the maximum tensile Z-strain and compressive X-strain on the ship resembled the effective stress, which increases during collisions with larger ice blocks. However, the tensile X-strain and compressive z-strain had varying trends; Appendix B.

lists the figures. The next study determined how increasing the number of ice cubes in the field affected the ship.

C. INCREASING NUMBER OF ICE CUBES

In this parametric study, the number of ice cubes in the fluid field increased from one cube, to three, to five cubes. The user expected that adding ice cubes to the fluid field would result in higher effective stress and strain. For all of the tests, the ice was submerged by 90% and the ship had a 5 m/s velocity. Figure 41 illustrates the maximum effective stress on the ship.

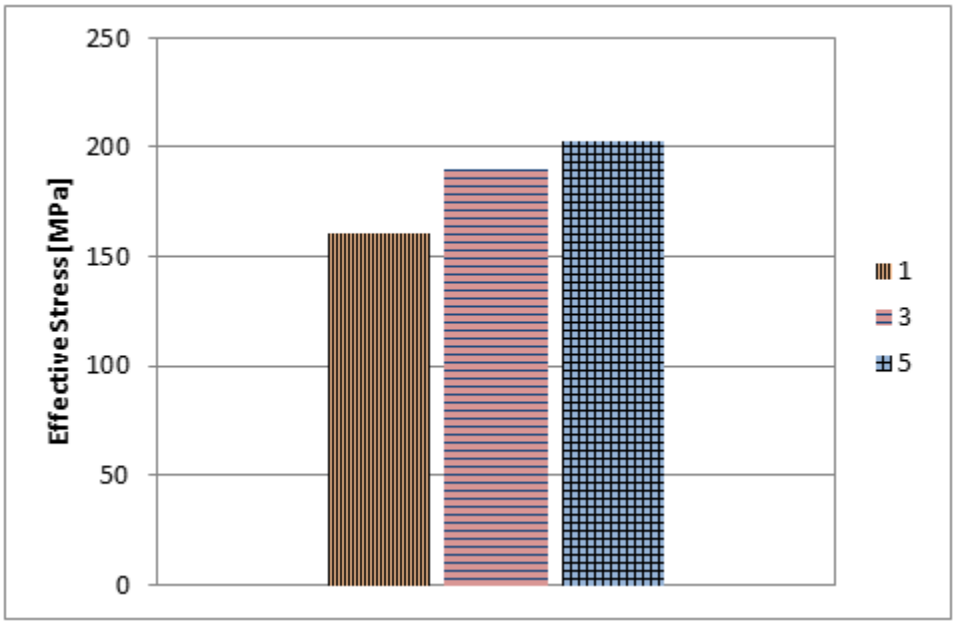

Figure 41. Effective Stresses for Number of Ice Cubes

Figure 41 shows that adding ice cubes directly correlates to increases in the maximum effective stress. Note that the change in effective stress between one and five ice cubes is minimal considering the five times increase in the number of cubes. Figure 42 and Figure 43 provide graphics of the three and five block simulation. Note that for both of these runs, only half of the simulation is visible. The other half of the simulation

is on the other side of the fluid domain. Therefore, only 1.5 of the three and 2.5 of the five ice cubes appear in Figure 42 and Figure 43, respectively.

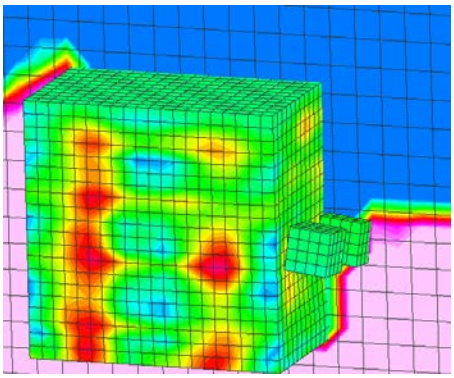

Figure 42. Graphic for 3 Ice Cubes

In Figure 42, the maximum effective stress is found at 199.7 msec. For the structure, the minimum velocity is 0.494 m/s and the maximum velocity is 22.3 m/s. For the fluid, density is shown. The minimum density is 0.00 g/cm3 and the maximum density is 1.0 g/ cm^3.

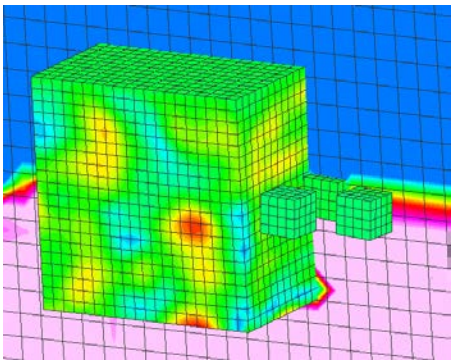

Figure 43. Graphic for 5 Ice Cubes

In Figure 43, the maximum effective stress is found at 148.1 msec. For the structure, the minimum velocity is 0.261 m/s and the maximum velocity is 21.4 m/s. For the fluid, density is shown. The minimum density is 0.00 g/cm3 and the maximum density is 1.0 g/ cm^3.

In the three block test, all the ice cubes collided with the ship. However, in the five block test, the two blocks further from the hull do not collide with the ship. The bow wake pushes the two blocks away from the ship, shown in Figure 43. Even though the two ice blocks do not collide with the hull, they still impact the maximum effective stress, as graphed in Figure 44. Appendix B. lists the X and Z strain graphs for the number of ice cube test. After varying the ship speed, ice cube size, and number of ice cubes, the next test manipulated the hull shape. The following section analyzed tumblehome, flared, and vertical hulls.

D. VARYING SHIP HULL

The previous parametric studies conducted tests on a vertical hull. This section compares the stress and strain on a vertical hull, a tumblehome hull, illustrated in Figure 21, and a flared hull, shown in Figure 22. For these tests, the ship maintained a constant 5 m/s velocity and the ice cube had a 5 cm edges. Figure 44 shows the maximum effective stresses on all three hulls.

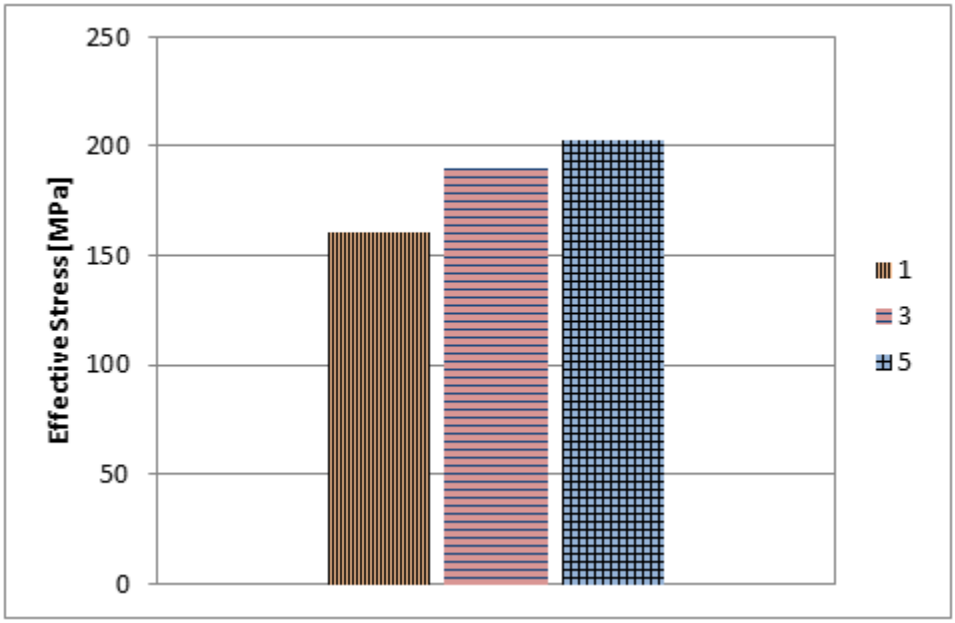

Figure 44. Effective Stresses for Hull Shapes

It was expected that the tumblehome hull would have the lowest maximum effective stress because it is more hydrodynamic. The quantitative data agrees with this assumption, revealing that the stress on the tumblehome hull is 52% of the maximum effective stress of the vertical hull and 69% the stress of the flared hull. Figure 45 through Figure 47 provide graphics of the numerical simulation when measuring the maximum effective stress.

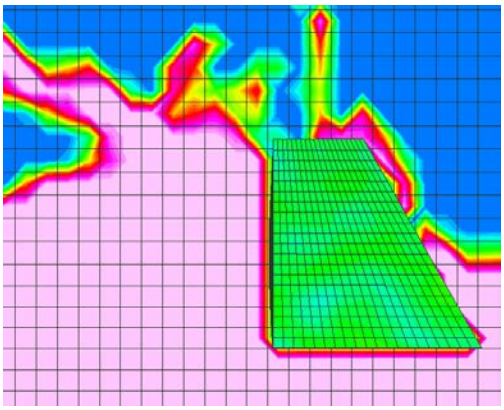

Figure 45. Graphic for Tumblehome Hull

In Figure 45, the maximum effective stress is found at 182.9 msec. For the structure, the minimum velocity is 0.229 m/s and the maximum velocity is 12.4 m/s. For the fluid, the minimum velocity is 0.00 m/s and the maximum velocity 14.3 m/s.

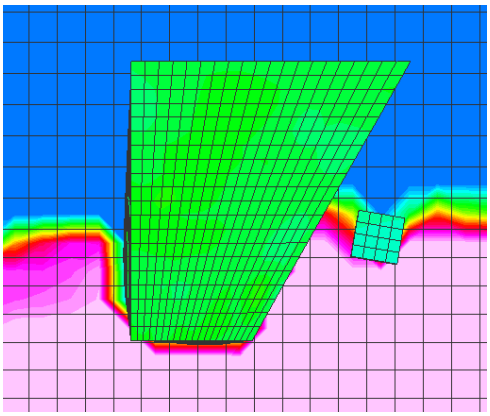

Figure 46. Graphic for Flared Hull

In Figure 46, the maximum effective stress is found at 27.5 msec. For the structure, the minimum velocity is 0.229 m/s and the maximum velocity is 8.57 m/s. For the fluid, the minimum velocity is 0.00 m/s and the maximum velocity 7.09 m/s.

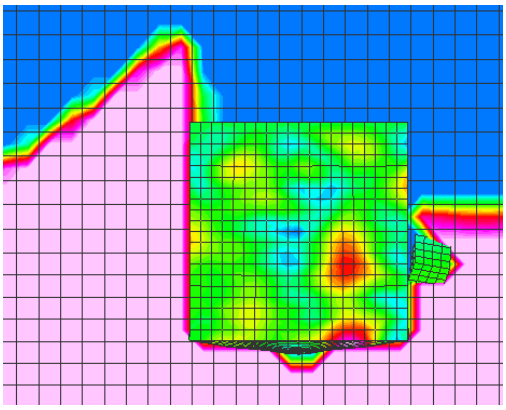

Figure 47. Graphic for Vertical Hull

In Figure 47, the maximum effective stress is found at 199 msec. For the structure, the minimum velocity is 0.561 m/s and the maximum velocity is 18.3 m/s. For the fluid, the minimum velocity is 0.00 m/s and the maximum velocity 23.7 m/s.

Figure 45 shows that a very large bow wake causes the water to move upward. This upward bow wake pushes the ice cube up and out of the fluid field; thus, the effective stress on the hull is primarily from the bow wake instead of being from the ice block. For the flared hull in Figure 46, the hull shape pushes the water downward into the vertical water column. The ice block is pushed in front of the ship hull. In Figure 47, the vertical hull also pushes the ice cube around, and the flat surface creates a high amount of drag on the surface.

The water movement around the hull shown in Figure 45 through Figure 47 corresponds to the effective stress on the hull. Due to the high drag, the vertical hull has the highest effective stress and the hydrodynamic tumblehome hull yields the lowest effective drag. In regards to reducing the maximum effective stress, it is clear that the tumblehome is the most ideal geometry between the three tested hull shapes. Appendix B. lists the strain graphs for this parametric study.

THIS PAGE INTENTIONALLY LEFT BLANK

IV. METHODOLOGY: EXPERIMENTAL MODELING

In addition to running the numerical simulations, the researcher built a wave maker in the NPS tow tank. The researcher built and calibrated the equipment, but did not run tests that could be used to validate DYSMAS results. This chapter provides an overview of basic wave theory, types of wave generating systems, and the wave maker design process.

A. WAVE THEORY AND MOTION

This section covers linear wave theory, non-linear wave theory, and wave particle motion. Wave theory is pertinent to this thesis because the researcher designed and built a wave generating system.

1. Linear Waves

Linear wave theory is the foundation of coastal and naval engineering. A linear, or regular, wave moves in a sinusoidal motion and has constant height, length, and period. Wave generator can easily generate regular waves in the controlled laboratory environment. Note that regular waves are defined in both the temporal or spatial domains, as shown in Figure 48.

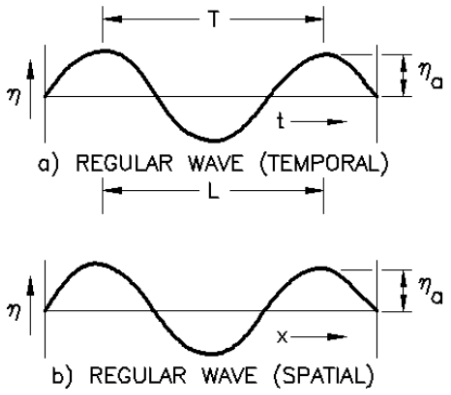

Figure 48. Representation of a Regular Wave. Source: [24].

While regular, sinusoidal waves help explain wave motion, they are not an accurate representation of nature. As observed from visual inspection, the sea surface moves in an irregular manner with varying wave heights, periods, and speeds. These types of waves are non-linear and are covered in the following section.

2. Non-linear Waves

Irregular, or non-linear, waves accurately represent ocean waves and form through the superposition of component regular waves, as illustrated in Figure 49.

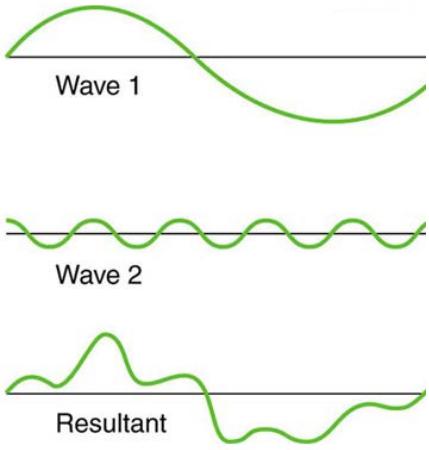

Figure 49. Superposition of Regular Waves to Form Irregular Wave. Source: [25].

Each component linear wave has its own speed and height. As multiple linear component waves superpose, the shape of the irregular waves becomes more complex. The irregular wave is also constantly changing with time because linear waves pass through irregular waves with varying velocities and wave heights.

3. Wave Particle Motion

In addition to linear and non-linear waves, water particle motion is fundamental to wave theory. Ocean engineers use the ratio of the water depth, d, and the wave length, L, to categorize waves as deep water, transitional (intermediate), or shallow waves. Depending on the category, the water particle motion changes, as shown in Figure 50.

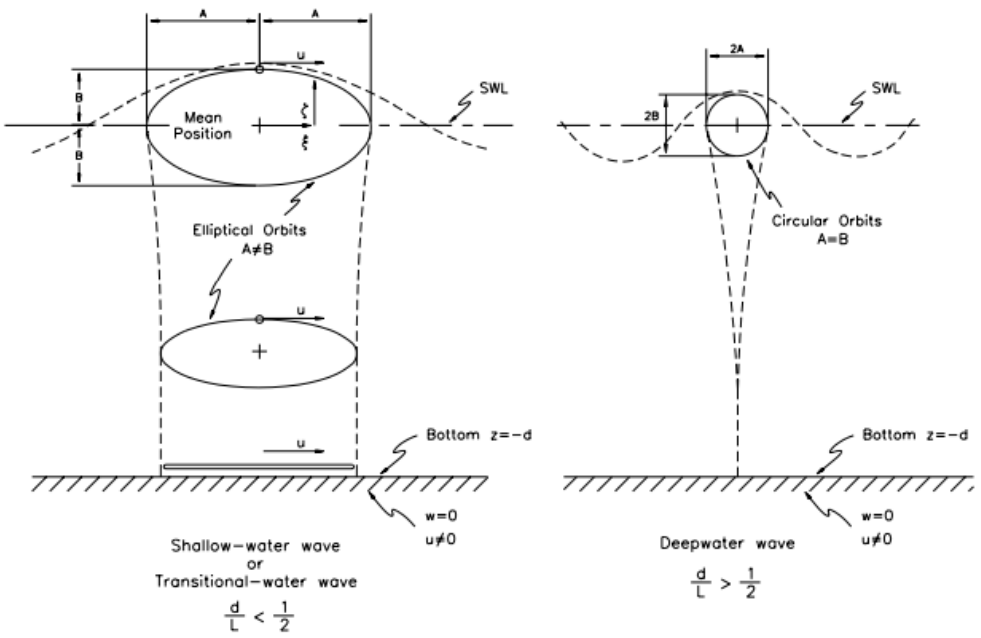

Figure 50. Wave Particle Motion. Source: [24].

Figure 50 demonstrates that shallow and transitional wave particles orbit elliptically while deep water waves move circularly. Laboratory wave generation systems produce different types of water particle motion. Therefore, the experimenter should know the generated wave profile while conducting experiments on ships and structures.

B. WAVE GENERATOR DESIGNS

Wave generators replicate controlled ocean environments, which helps experimenters test and validate computational results from ships and naval structures. These tanks replicate two-dimensional progressive wave trains, enabling experimenters to measure the dynamic response and motion of structures. Wave generators are beneficial because they are a fraction of the cost compared to actual sea trials. The three primary systems of wave generators are plungers, pistons, and flappers. These generators produce waves by pushing a plate or wedge. The speed and distance the plate or wedge moves affects the wave height and period.

A popular wave system is the plunger design, which oscillates vertically. The plunger is best at simulating deep-water waves that have circular underwater particle motion [26]. The vertical plunger is theoretically more complex than the horizontal wave maker because it changes the volume of the fluid, yielding non-linear effects [27]. Therefore, experimental tests are required to determine the wave conditions and particle motion for each tank. Figure 51 shows a typical plunger wave maker.

Figure 51. Plunger Wave Generator. Source: [28].

A paddle wave maker, as depicted in Figure 52, is hinged to the tank floor and is best at producing transitional wave motion that has elliptical particle motion [26]. The third type of system, piston wave makers, moves horizontally and replicates shallow waves that have ovular particle motion [26]. Figure 53 illustrates a piston wave maker. These three types of wave systems are the most common, but other complex systems move translationally and rotationally to replicate a wide range of water depths.

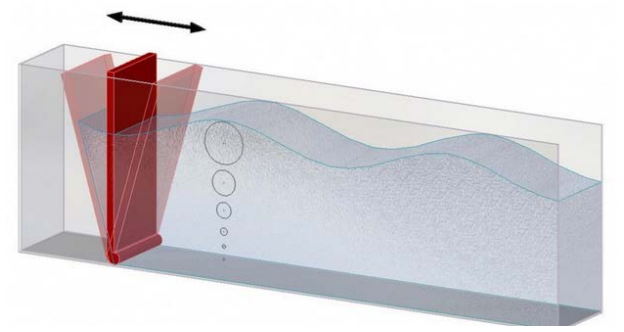

Figure 52. Paddle Wave Generator. Source: [29].

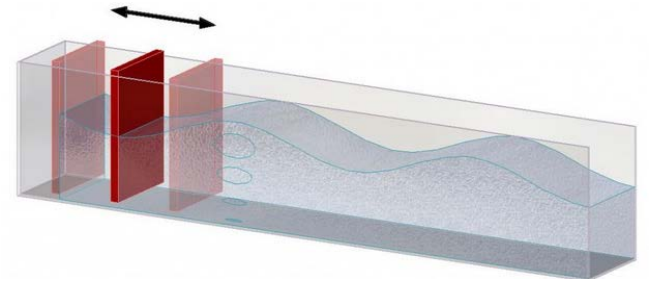

Figure 53. Piston wave Generator. Source: [29].

C. DESIGNING NAVAL POSTGRADUATE SCHOOL WAVE TANK

NPS has an existing tow tank that can model the movement of offshore structures and vessels. The tow carriage pulls objects, such as ships and structures, through the tank in order to replicate hydrodynamic characteristics along the length and depth of the channel. NPS' tow tank is illustrated in Figure 54.

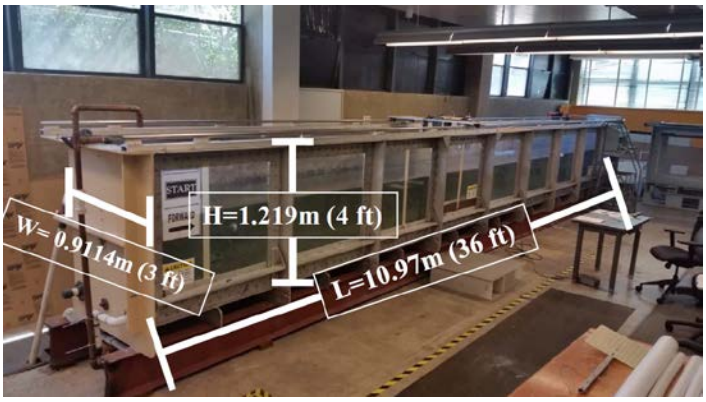

Figure 54. Halligan Hall Tow Tank. Source [11].

Objects are towed in the channel through a carriage system that spans the top of the tank. The carriage uses a five horse-power motor that is connected to a pulley system. The tow tank operator can input the carriage speed settings. The manual to operate the carriage is listed in the *Hydrodynamic Response of a Composite Structure in an Arctic Environment* [11]. The tow tank is not designed for wave generating capabilities, and thus, the researcher designed the wave system around the tow carriage.

1. Existing Wave Generation Systems

First, the researcher determined the appropriate wave generation system –plunger, flapper, or piston. The main design criterion was to minimize tank alterations. A piston system would require mechanics to be mounted inside the tank, resulting in major structural changes to the channel. The flapper system would also require tank alterations because flapper systems are connected to the channel floor. The frame of a plunger system could be built outside the tank and the plunging wedge could be suspended inside. Therefore, the researcher selected the plunger system because it results in the fewest tank modifications.

In addition to being the most ideal system, the plunger mechanism is used by the United States Naval Academy Hydrodynamic Laboratory. The Naval Academy's staff collaborated with the researcher to design the NPS wave maker. Multiple components of the NPS plunger design were based off of the Naval Academy's tank design, which is shown in Figure 55.

Figure 55. U.S. Naval Academy Plunger Wave Maker. Source: [30].

2. Linear Motion Mechanism

After selecting the wave generator system, the researcher determined the appropriate mechanism to vertically move the plunger. Initially, the researcher used the scotch-yoke mechanism The Scotch-Yoke mechanism is beneficial because it has few moving components, which reduces the likelihood of failing parts. The Scotch-Yoke mechanism is illustrated in Figure 56.

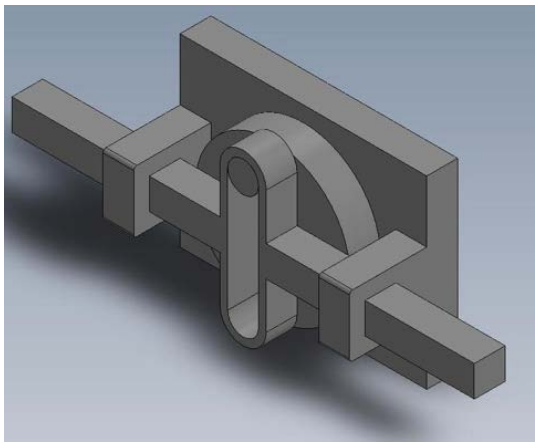

Figure 56. Scotch-Yoke Mechanism. Source: [31].

However, this system has several limitations. First, the linear distance of movement is fixed because the motion is dependent on the circumference of the wheel. Therefore, the circular motion can only create sinusoidal waves because the plunger motion is fixed. Second, the linear speed is restricted to the speed of the motor. Ultimately, the sinusoidal waves generated from the scotch-yoke mechanism limit the possibility of simulating non-linear waves.

Next, the researcher considered linear actuators that use either ball screws or acme screws. Ball screw actuators are more expensive than acme screw actuators, but they are able to operate at high speeds with great precision [32]. The operator uses a controller to manipulate the linear actuator's vertical movement and speed. Figure 57 is an image of the linear actuator.

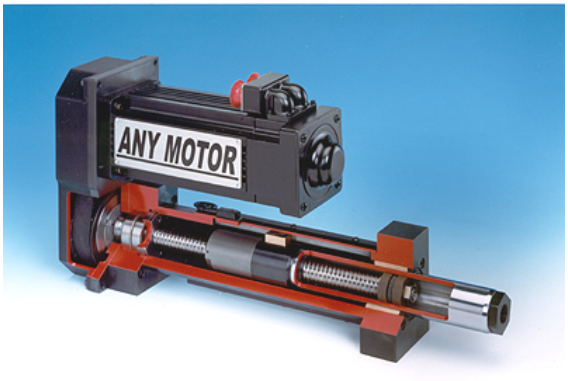

Figure 57. Linear Actuator. Source: [32].

A true non-linear wave is created by superposing linear waves. Unless the user creates a script or purchases commercial software to superpose linear waves, the actuator cannot generate irregular waves. However, the actuator can still replicate what appears to be a non-linear sea surface by creating multiple linear waves with varying the speeds and heights within a wave run. Thus, the researcher chose the ball screw linear actuator as the mechanical system for the wave tank because of the actuator's speed and stroke length flexibility.

3. Accommodating Wave Generator to Existing Tow Tank

This section provides information on why the researcher chose certain equipment and how the wave generating system was attached to the tank.

a. Equipment Selection

After selecting the linear actuator as the mechanical system, the researcher determined the desired speed and vertical distance of the plunger in the tank. The primary concern was to avoid interfering with the existing tow carriage mechanism. The safe operating height is 0.406 m (16 inches), and Appendix C provides figures that show how the researcher determined the stroke length.

Another selection criterion was the actuator's speed. Depending on cost, the selected actuator model may move up to 1.52 m/s (60 inches per second). However, the faster the actuator is, the more expensive is the cost. Therefore, the researcher chose a maximum operating speed of 0.406 m/s (16 inches per second), which allows the plunger to travel the stroke length in one second.

Next, the researcher designed and selected the material for the plunger. The plunger is built from 5086 aluminum sheets. The 5086 aluminum is marine aluminum, which is very corrosion resistant and can easily be welded. Therefore, the user selected 5086 even though it is approximately 30% more expensive than 6061 aluminum [33]. Figure 58 shows the constructed wedge, and a sketch with the dimensions is listed in Appendix C.

Figure 58. Aluminum Wedge

Additionally, the researcher needed to select the metal to build the wave generator frame. The main criterion was a material that could be quickly assembled and modified. At first, aluminum bars were considered, but this would require welding pieces of the frame together. Therefore, these bars were disregarded. The researcher considered 80/20 aluminum bars. The 80/20 bars have t-slots that allow the user to join pieces together through internal and external brackets. The 80/20 company also sells bearing systems and floor mounts. Once the pieces have been assembled, the user can still be modify the frame because welding is not required. Therefore, the researcher selected 80/20 aluminum bars, as shown in Figure 59. The purchase order for all of the 80/20 parts are listed in Appendix D.

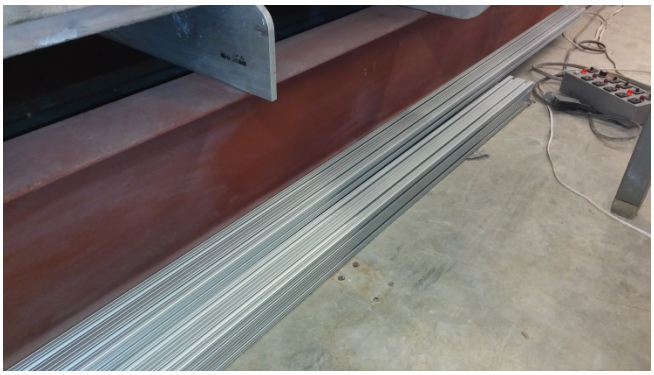

Figure 59. 80/20 Aluminum Bars

The final step was for the researcher to determine the linear actuator, the motor, and the controller to operate the system. The researcher collaborated with ModuSystems, Inc, which is a company located in Santa Clara, CA, to select the proper motor and controller for the linear actuator. An E-drive actuator was selected which has a 24” stroke, 400 lbs thrust, and 16 in/sec maximum velocity. The actuator is run by an Animatics Integrated Servo Motor and Amplifier and both systems are regulated with a ModuSystem Pulse/Dir Controller and Power Supply. The dimensions and specifications for the components are listed in Appendix E. Figure 60, Figure 61, and Figure 62 depict the components of the wave generating system.

Figure 60. Linear Actuator

Figure 61. Animatics Motor

Figure 62. Modusystems Controller

b. Designing the Wave Maker

After selecting all of the equipment, the researcher designed the wave generator in Solidworks. As stated previously, the main criterion was to avoid interfering with the tow carriage. Several components, such as the angle of the wedge, are modeled after the Naval Academy's wave tank. Figure 63 is a sketch of the finalized wave generator design.

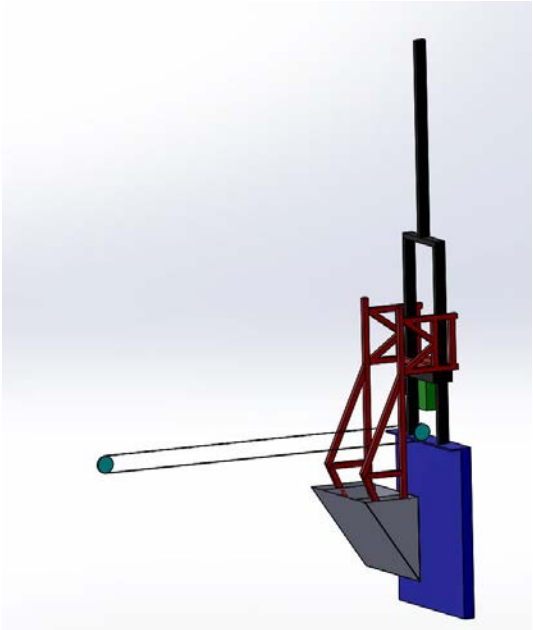

Color	**Part**	**Color**	**Part**
Turquoise	Tow Carriage	Red	Plunger frame
Purple	Channel Wall	Green	Linear actuator
Black	Mounting Frame	Gray	Wedge

Figure 63. Wave Generator Sketch

Figure 63 shows the wedge mounted to the red plunger frame. This red frame slides vertically on the black mounting frame along bearings. The green linear actuator is mounted to the black frame, and it propels the plunger frame vertically inside the channel to produce waves. The mounting frame has a black bar extending upward to the ceiling to provide additional support and stabilization due to the moment caused by the plunger.

D. BUILDING THE WAVE GENERATOR SYSTEM

The wave maker construction took place over several steps. The wave maker was mounted to the back of the tank flange, as shown in Figure 64. The first step was sanding down and drilling holes into the tank flange. This step is illustrated in Figure 65. The foot mounts for the generator were attached to the flanges and the posts were erected. The 80/ 20 aluminum bars were also cut for the tank frame, as shown in Figure 66 and Appendix E.

Figure 64. Location of Wave Generator Structure

Figure 65. Tank Flange

Figure 66. Wave Generator Frame

The machine shop cut brackets that join the 80/20 pieces, as shown in Appendix E. The author of this thesis also assembled and tested the linear actuator, motor, and controller. During the time of thesis submission, public works closed the NPS tow tank spaces for environmental characterization of asbestos, as shown in Figure 67.

Figure 67. Halligan Hall Closure

The closure impacted the wave generator construction. However, the researcher salvaged the parts left in Halligan Hall and continued to construct the generator. Once the building is re-opened, the final step is to attach the components to the tank. The final assembly of the wave generator is not shown in this thesis.

THIS PAGE INTENTIONALLY LEFT BLANK

V. CONCLUSION AND REVIEW

The author of this thesis accomplished the numerical and experimental goals of the project. The purpose of the numerical study was to determine how composite-hull ships behave in Arctic conditions. The findings from the parametric study revealed that increasing the ship velocity, enhancing the ice block size, and expanding ice blocks field all resulted in a larger maximum effective stress on the ship hull. Through geometric similitude, one may use Froude or Reynolds number to scale the results of these tests to a real model. The ship velocity test provided the most interesting results, which was analyzed with and without ice blocks. The data showed the position at which the ice block strikes the ship has a greater influence on the maximum stress. However, the velocity test had unexpected outcomes because simulations without ice had higher effective stresses than tests with ice. The ship was built as a thin elastic shell that experienced a lot of bending and compression. When the ice collided with the ship, it provided resistive loading from the fluid dynamics, thus decreasing the effective stress on the hull. The numerical study also examined tumblehome, flared, and vertical hulls. The tests revealed that the ship hull angle influenced the fluid flow, which in turn affected the ice block position. The vertical, flared, and tumblehome hulls had the highest to lowest maximum effective stress, respectively. This thesis provided quantitative effective stress trends for each parametric study that establishes the relationship between composite-hulls interacting with ice.

The experimental objective to design a wave generating system was completed, but the final assembly of the system is still in progress at the time of this thesis submission. The wave system was designed, the parts were purchased, and the construction was almost complete. However, an unexpected closure due to an environmental characterization of asbestos shut down the Halligan Hall tow tank spaces. This prevented the researcher to fully assemble the wave generating system. Regardless, the researcher still cut and assembled the major components for the wave generator, leaving the mounting process as the final step.

The researcher faced several obstacles during the wave generator design phase. There was limited safe operating stroke length for the plunging wedge because the tow carriage spanned across the entire channel, creating an obstacle for the wave generator. The researcher designed a system that operated around the generator while maintaining a safe distance from the tow carriage. There were also electrical limitations because the motor operates off of 220V, but only 110V are readily accessible in the tow tank spaces. Therefore, a power supply was used to step down the voltage to avoid new electrical wiring. Despite these numerical and experimental limitations, alternative methods addressed these obstacles.

Due to the limited time period of this thesis, several numerical and experimental targets were not completed. However, these objectives may be completed in future research efforts. Waves could be added to the DYSMAS simulations to realistically model ocean conditions. DYSMAS does not have a preset function to produce surface waves. Therefore, future projects may test if a large wedge could be elevated above the fluid surface and accelerated into the water to create waves. This simulation would replicate how waves are experimentally generated in the wave tank. This numerical test would allow the researcher to test ships interacting with ice while transiting through ice. The numerical results could then be confirmed experimentally in the wave tank. In addition to the numerical wave generation, the ship hull could also be built as a rigid material instead of an elastic shell to reduce structural bending. The ship and ice could also be increased to model full scale vessels.

Experimentally, another researcher could calibrate and finalize the Halligan Hall tow tank once the wave generating system is fully built. A future researcher could tabulate the generated wave heights when the wedge operates at different stroke lengths and speeds. Honeycomb wave breaking material should also be built at the opposing side of the channel to reduce wave reflection during experiments. Additionally, wave particle motion should be analyzed to determine if the wave system produces deep, transitional, or shallow waves.

The thesis has implications for the U.S. Navy both computationally and experimentally. The trends from the numerical modeling provide the foundation to future

composite research in the DYSMAS program. The Halligan Hall wave tank creates opportunity for future experimental wave research, which was not previously possible at NPS. As sea lanes continue to open up north, the Navy must continue with composite-hull research to ensure dominance in the emerging Arctic frontier.

THIS PAGE INTENTIONALLY LEFT BLANK

APPENDIX A

Equation of State for Fluid Materials. Source: [34].

Material	Air		
EOS Type	Gamma-Law		
Equation	$p = (\gamma - 1)\rho e$		
Material Property			Units
Reference Density	ρ_{ref}	0.0013	g/cm^3
Reference Specific Energy	e_{ref}	1.9230769E+09	erg/g
Reference Speed of Sound	c_{ref}	3.28E+04	cm/s
Minimum Density	ρ_{min}	1.0d-06	g/cm^3
Minimum Specific Energy	e_{min}	1.0d-4	erg/g
Gamma	γ	1.4	N/A

Material	Water		
EOS Type	Tillotson		
Equation	$p = p_o + \omega\rho(e - e_o) + A\mu + B\mu^2 + C\mu^3$ where $\mu = \frac{\rho}{\rho_o} - 1$		
Material Property			Units
Reference Density	ρ_{ref}	1	g/cm^3
Reference Specific Energy	e_{ref}	3.54E+09	erg/g
Reference Speed of Sound	c_{ref}	147600	cm/s
Minimum Density	ρ_{min}	9.999E-03	g/cm^3
Minimum Specific Energy	e_{min}	-9.999E+10	erg/g
Minimum Pressure	p_{min}	50000	$dyne/cm^2$
Omega	ω	2.80E-01	N/A
Constant	A	2.20E+10	N/A
Constant	B	9.54E+10	N/A
Constant	C	1.457E+11	N/A

THIS PAGE INTENTIONALLY LEFT BLANK

APPENDIX B

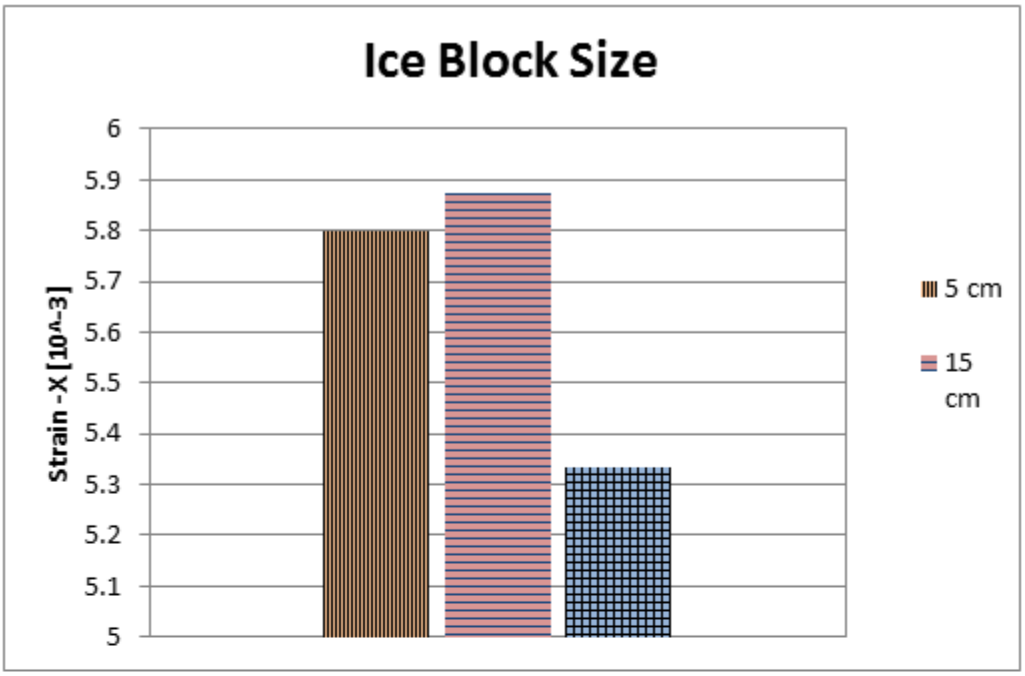
Ice Block Size
Strain -X [10^-3]
6
5.9
5.8
5.7
5.6
5.5
5.4
5.3
5.2
5.1
5
5 cm
15 cm

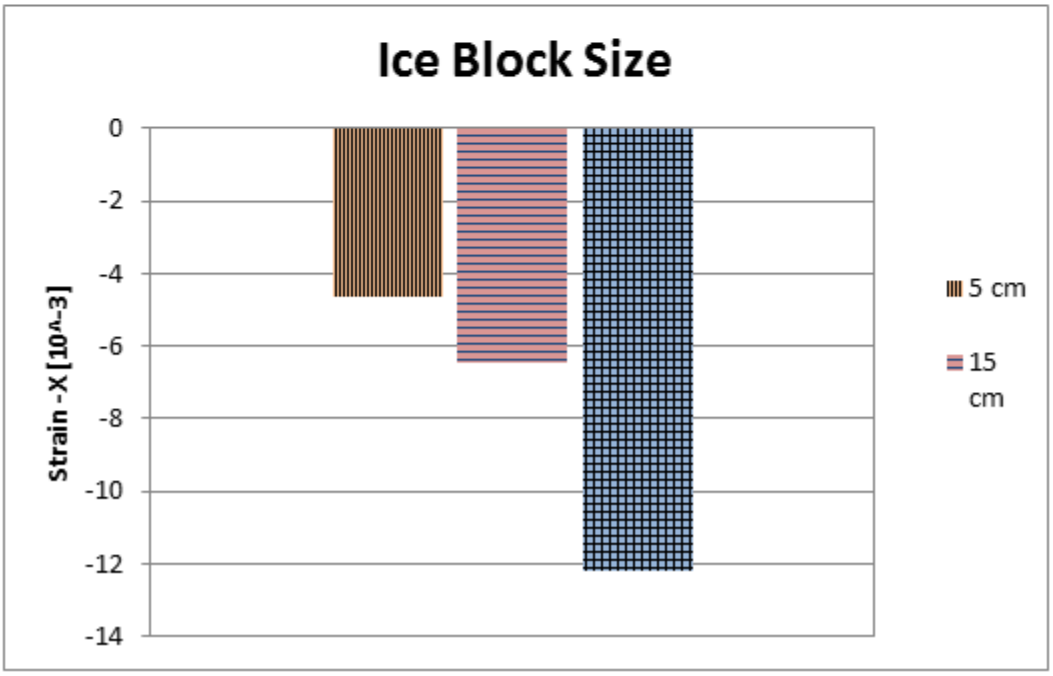
Ice Block Size
Strain -X [10^-3]
0
-2
-4
-6
-8
-10
-12
-14
5 cm
15 cm

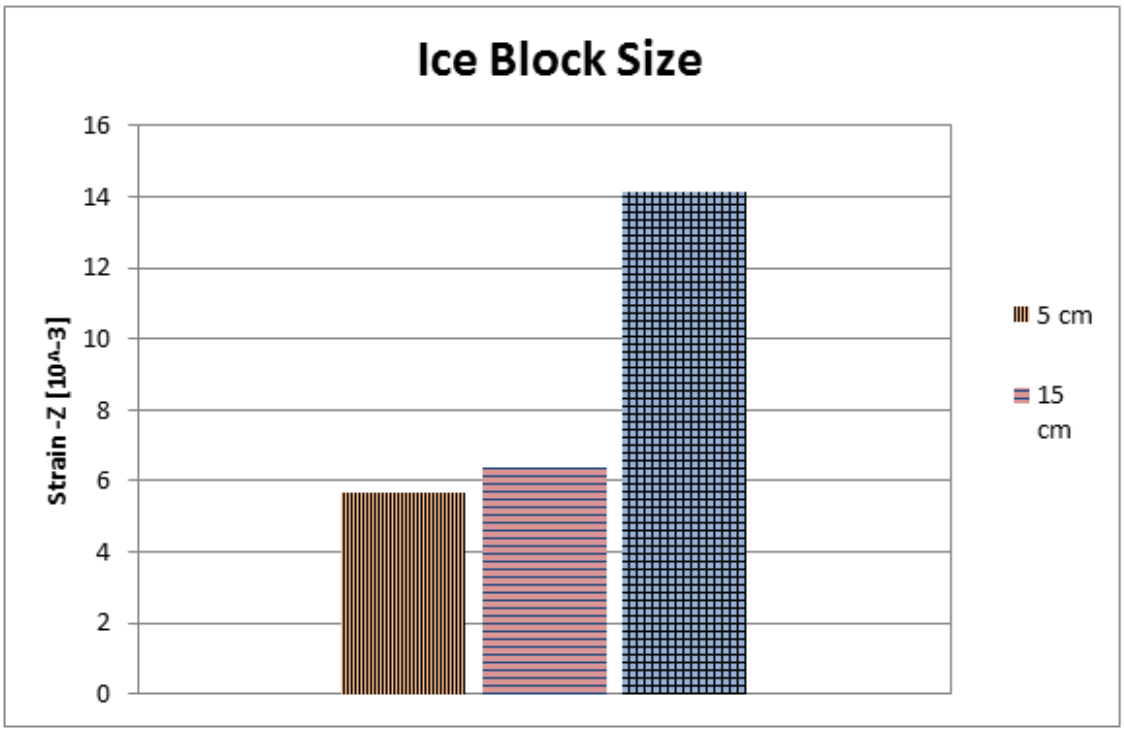
Ice Block Size
Strain -Z [10^-3]
16
14
12
10
8
6
4
2
0
5 cm
15 cm

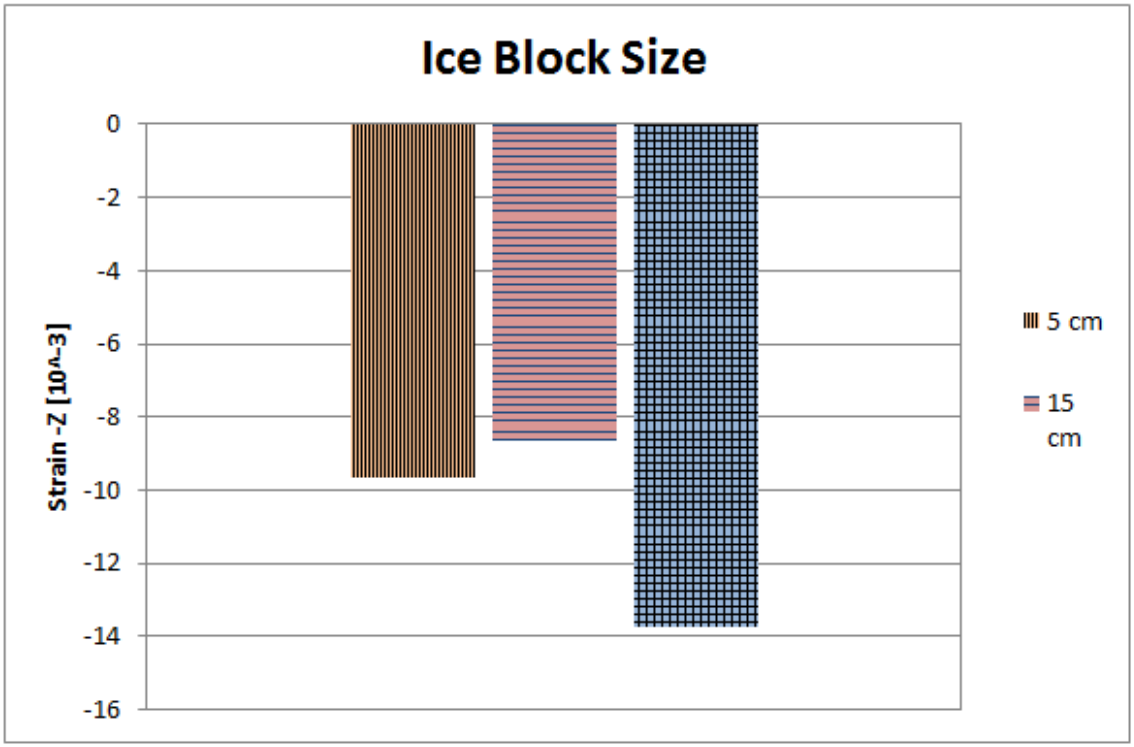
Ice Block Size
Strain -Z [10^-3]
0
-2
-4
-6
-8
-10
-12
-14
-16
5 cm
15 cm

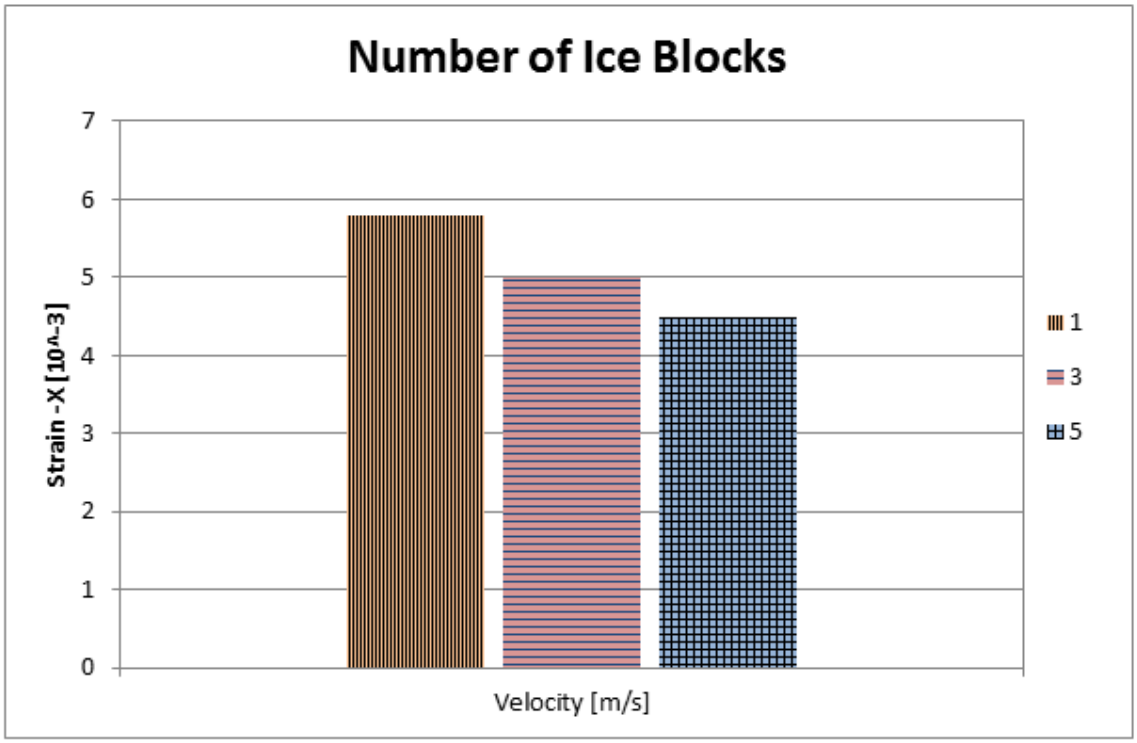
Number of Ice Blocks
Strain -X [10^-3]
7
6
5
4
3
2
1
0
Velocity [m/s]
1
3
5

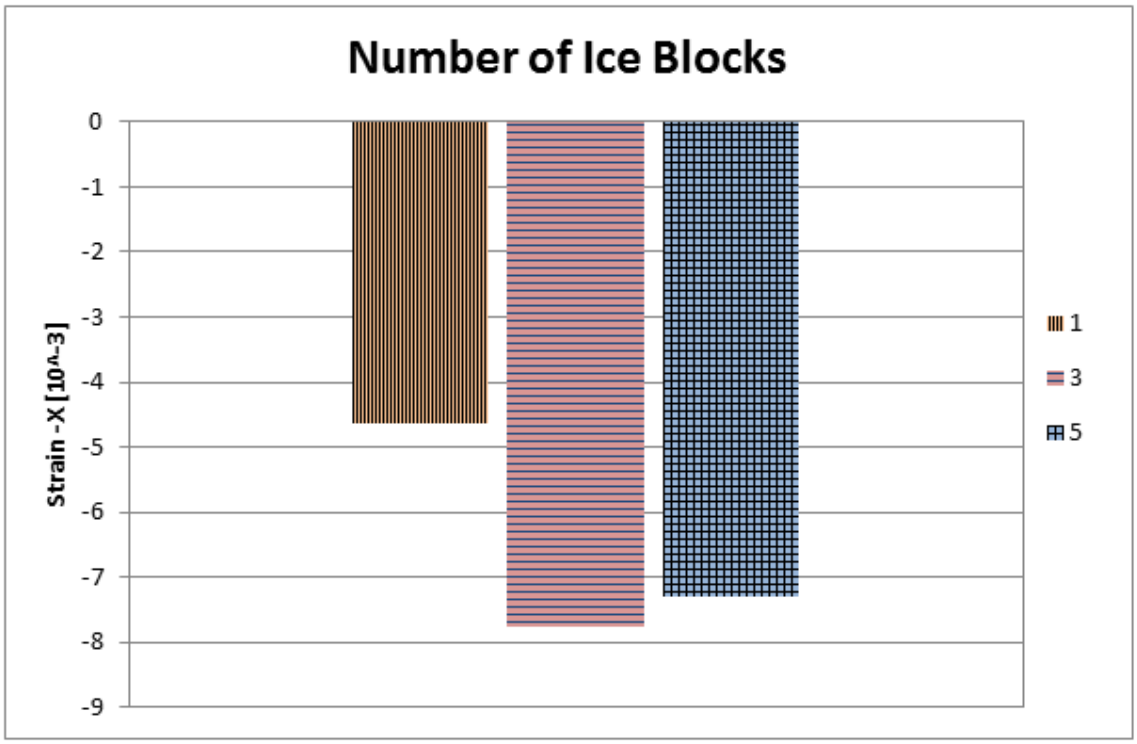
Number of Ice Blocks
Strain -X [10^-3]
0
-1
-2
-3
-4
-5
-6
-7
-8
-9
1
3
5

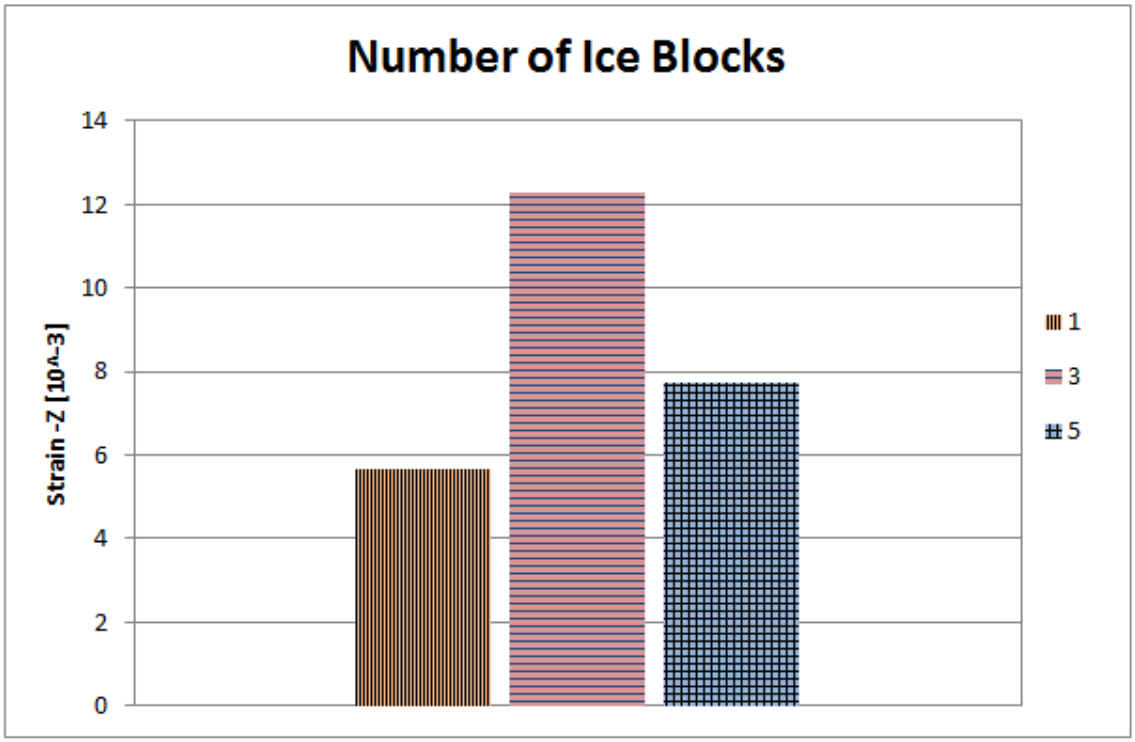
Number of Ice Blocks
Strain -Z [10^-3]
14
12
10
8
6
4
2
0
1
3
5

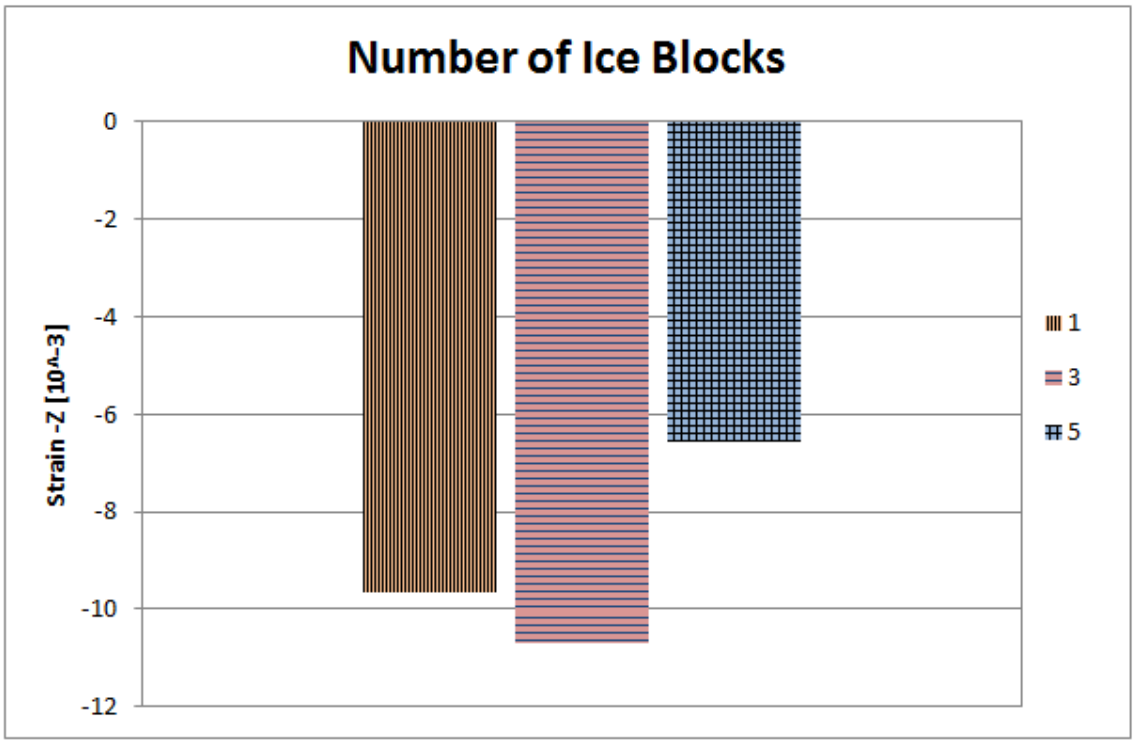
Number of Ice Blocks
Strain -Z [10^-3]
0
-2
-4
-6
-8
-10
-12
1
3
5

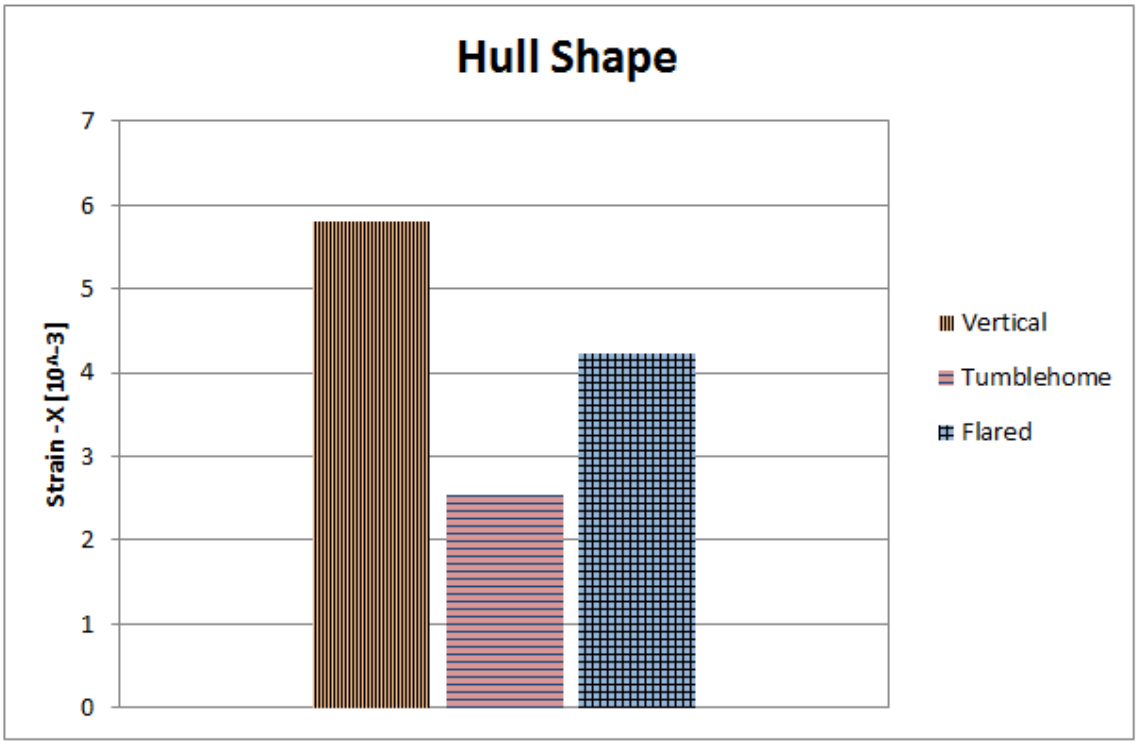
Hull Shape
Strain - X [10^-3]
7
6
5
4
3
2
1
0
Vertical
Tumblehome
Flared

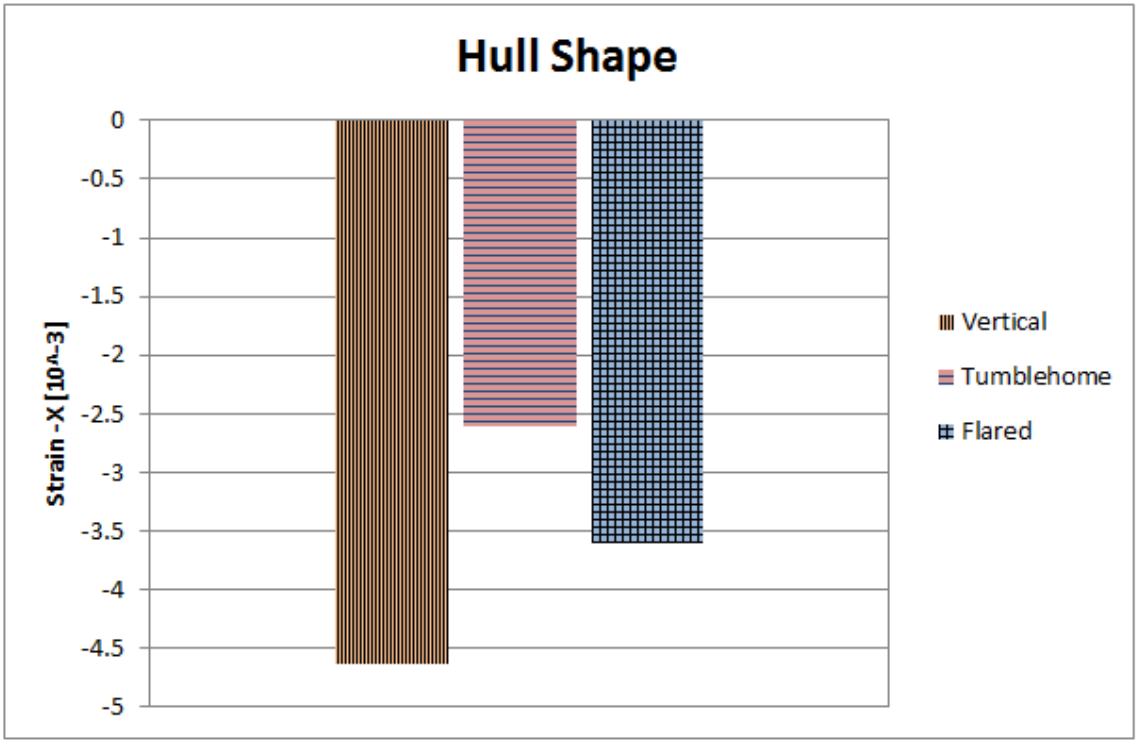
Hull Shape
Strain - X [10^-3]
0
-0.5
-1
-1.5
-2
-2.5
-3
-3.5
-4
-4.5
-5
Vertical
Tumblehome
Flared

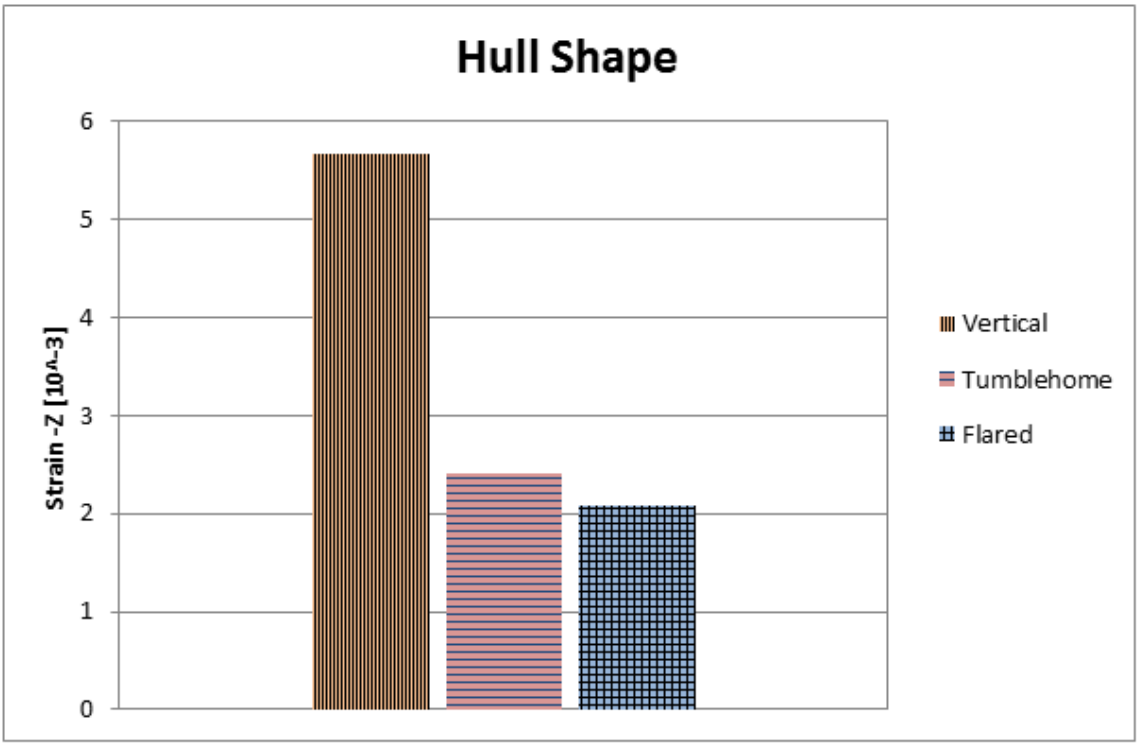
Hull Shape
Strain -Z [10^-3]
6
5
4
3
2
1
0
Vertical
Tumblehome
Flared

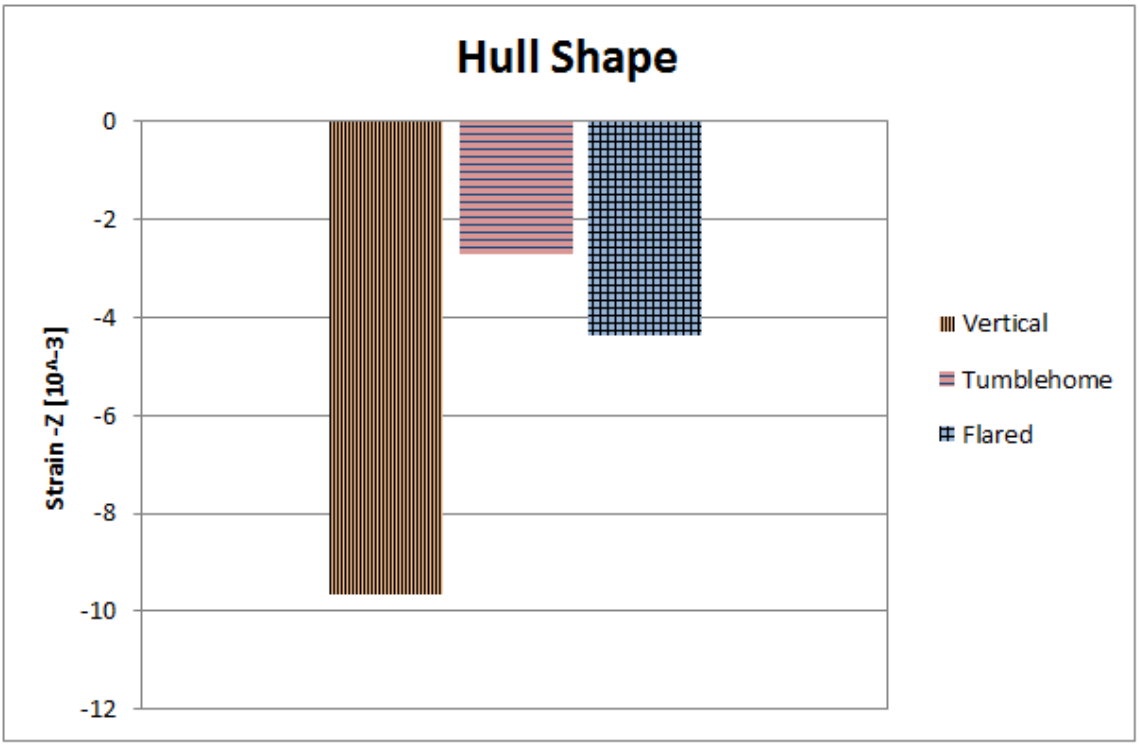
Hull Shape
Strain -Z [10^-3]
0
-2
-4
-6
-8
-10
-12
Vertical
Tumblehome
Flared

APPENDIX C

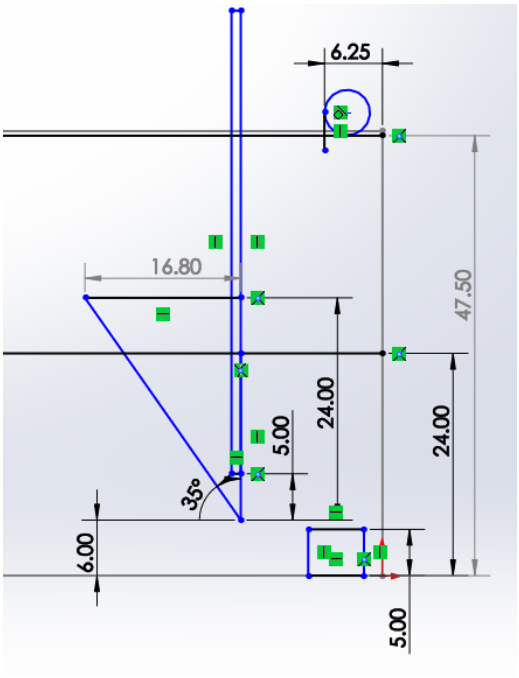

Full Stroke

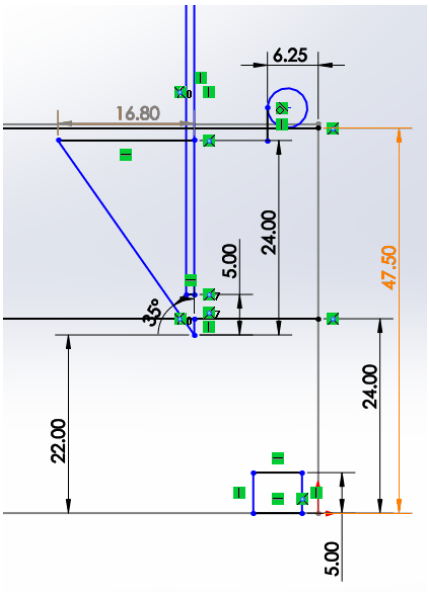

Minimum Stroke

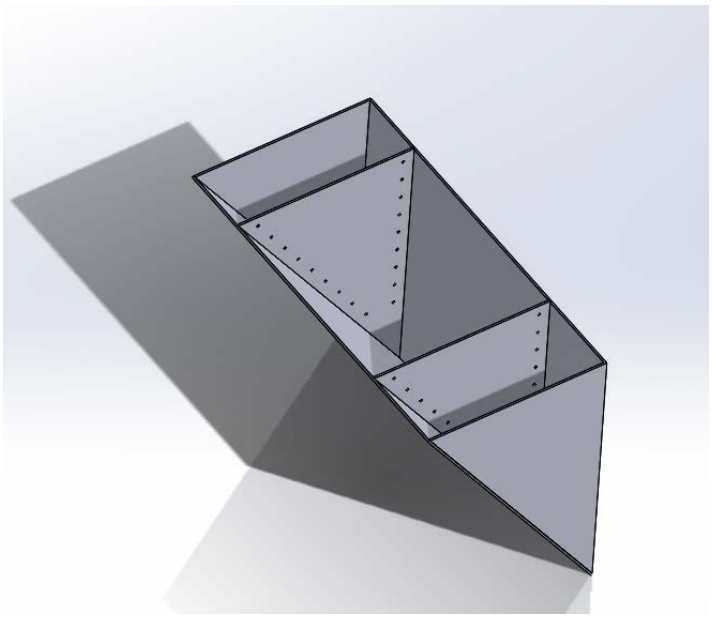

Aluminum Wedge

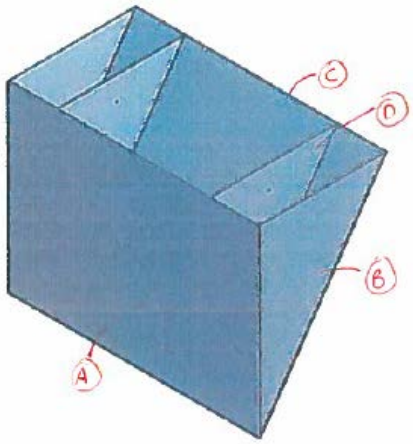

A - Back panel - Qyt: 1
B - Side Panel - Qyt: 2
C - Front Panel - Qyt: 1
D - Interior Panel - Qyt: 2

Materials Provided
QTY - 1 : 24 x 36"
QTY - 2 : 24 x 24"
QTY - 1 : 36 x 36"

A - Back Panel

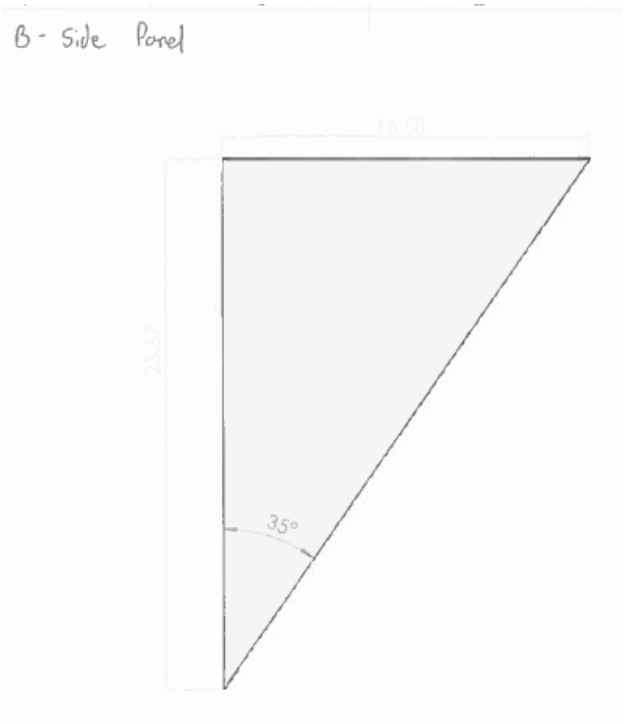
B - Side Panel
16.58
29.67
35°

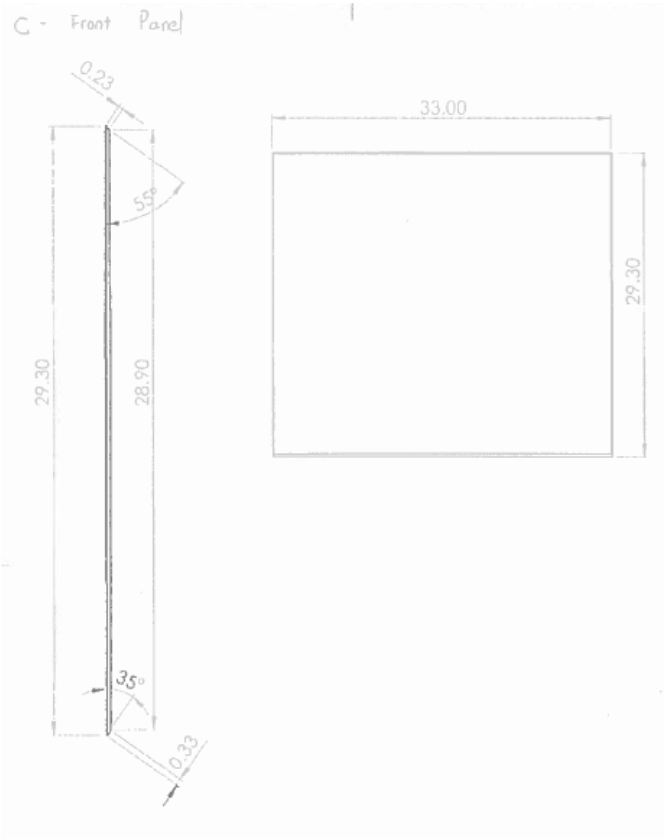
C - Front Panel
0.23
55°
33.00
29.30
29.30
28.90
35°
0.33

D - Interior Panel

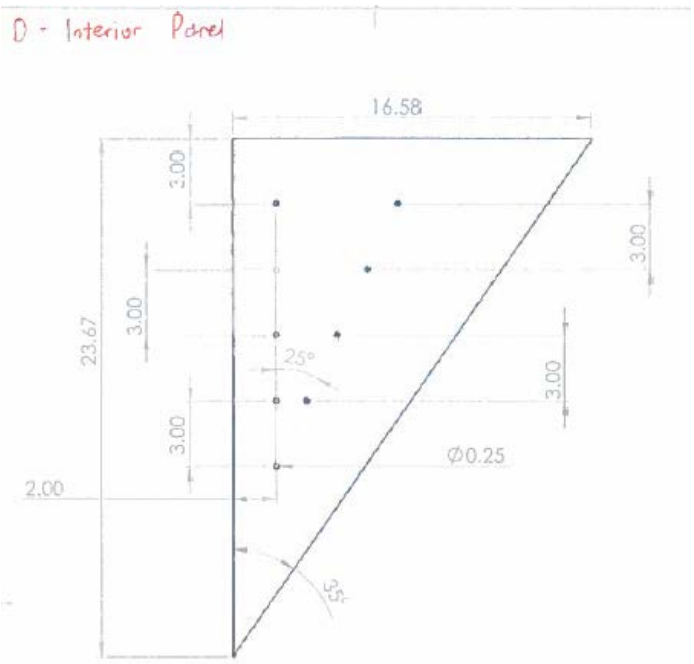

Note: All holes are ~~ϕ 0.25" counter~~
Ø.261

Top view

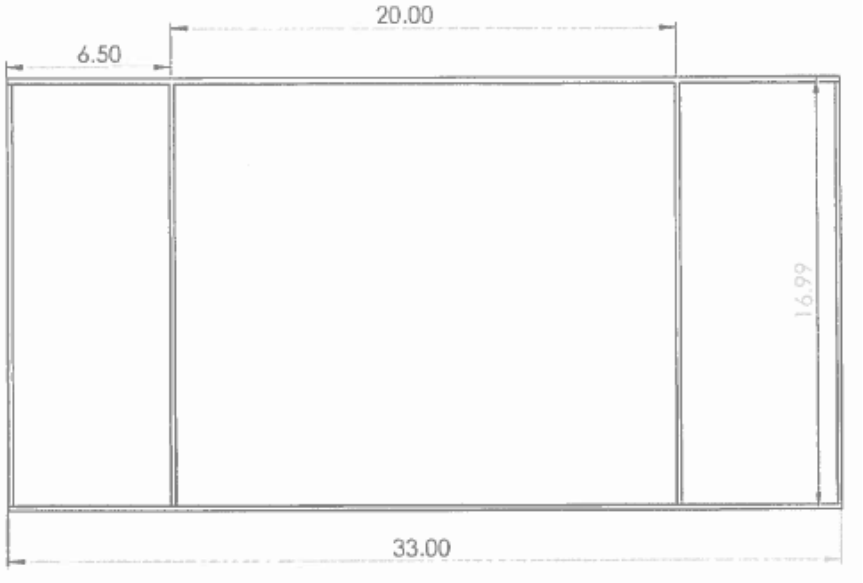

THIS PAGE INTENTIONALLY LEFT BLANK

APPENDIX D

80/20 Purchase Order

Wedge Support Arm					
	Description	FoS	Quantity	total (inch)	Part
A	73" Ultralite	75	2	150	1515-UL
B	36" Ultralite	36	2	72	1515-UL
C	11" Ultralite	12	2	24	1515-UL
D	30" Ultralite	32	2	64	1515-UL

Linear Actuator Arm					
	Description	FoS	Quantity	total (inch)	Part
A	13"	16	4	64	1515-UL
B	17"	20	4	80	1515-UL
C	12"	14	4	56	1515-UL
D	20"	22	2	44	1515-UL

Frame					
	Description	FoS	Quantity	total (inch)	Part
Base Plate	tank to frame		2		2410
Bearings	rollers		4		6834
Rail Frame	56"	60	2	120	3030
Top Rail Frame	50"	50	1	50	1530
Cross bars	23"	26	3	78	1530

Fasteners		
Description	Quantity	Part
Frame Cross bar support double	4	4338
Frame Cross bar support single	4	4334
Arm 90 deg connector single	8	4336
Arm 90 deg connector double	16	4332
5/16-18 Slide-in T-Nut (Single)	180	3278
5/16 Slide-in T-Nut (double)	20	3273
5/16-18 Flanged Socket Cap Screw	200	3330

LINEAR INDUSTRIES LTD.®
1850 Enterprise Way, Monrovia, CA 91016
(626) 303-1130 Fax (626) 303-2035

Item	Qty	Part #	Description
1	1	LS204-24-FF-M-U1-20-A01/SM34165MT	Model LS204-24-FF-M-U1-20-A01/SM34165MT Heavy Duty linear actuator including: a) 24 inch stroke b) 400 lb. thrust capacity c) 16 inch per second maximum velocity d) 0.500" diameter Ball screw; 0.500" lead e) 0.003"/foot lead accuracy; Backlash 0.004" (max) f) Dynamic capacity (*B10) of ball screw / ball screw support bearing system: 850 lb. for 1,000,000 inches g) Rugged Internal piston rod anti-rotation h) Internal magnet and switch mounting track i) Precision pre-loaded ball screw support bearings j) Parallel offset motor mount; 2:1 gear belt ratio k) To suit customer supplied servo motor / Animatics SM34165MT l) One (1) Normally Closed NC Hall Sourcing PNP Switches m) Front flange mount n) Male thread on rod end o) Air purge provisions p) Grease lubrication with re-grease provisions

STEVEN ENGINEERING
230 Ryan Way · South San Francisco · California 94080-6308
Main Office 650-588-9200
Outside Local Area 800-258-9200
Sales Fax 888-258-9200
E-Mail sales@steveneng.com

LINE NO.	ITEM NUMBER / DESCRIPTION
1	SM34165MT-IP Moog - Animatics MT Motors LOCAL STOCK
2	CBLIP-PWR4-FL-3M Moog - Animatrics LOCAL STOCK
3	CBLIP-IO-FL-3M Moog - Animatics LOCAL STOCK
4	CBLIP-COM-FL-3M Moog - Animatics LOCAL STOCK

ModuSystems

Animatics Integrated Servo Motor + Amplifier (IP67 Rated):
SM34165MT-IP
CBLIP-PWR4-FL-3M
CBLIP-IO-FL-3M
CBLIP-COM-FL-3M

L-TAC LS™ Linear Actuator Capabilities:

Model Number	Thrust Load Rated (lb_f)	Linear Velocity Max. (in/sec)	Travel Length[1] Max. (in)	Frame Size (in)	Lead[2] (in)	Ball Screw Diameter (in)	Ball Screw Max. (RPM)	Torque @ Ball Screw Max. (in-lb)	Dynamic Capacity per million revs (lb_f)	Dynamic Capacity per million inches (lb_f)	Motor Gearhead Frame Supported Max. (in)	Unit Weight "U" Motor Mount (lb)	Unit Weight "L" Motor Mount (lb)
LS204-24	400	16	24	2.25	0.50	0.50	1,920	35	1,070	850	3.5	15.0	13.5
LS204-30	400	11	30	2.25	0.50	0.50	1,320	35	1,070	850	3.5	18.0	16.5
LS204-36	400	8	36	2.25	0.50	0.50	960	35	1,070	850	3.5	21.0	19.5
LS209-24	900	9	24	2.25	0.20	0.63	2,700	32	1,070	850	3.5	15.0	13.5
LS209-30	900	8	30	2.25	0.20	0.63	2,400	32	1,070	850	3.5	18.0	16.5
LS209-36	900	5	36	2.25	0.20	0.63	1,500	32	1,070	850	3.5	21.0	19.5
LS305-30	500	40	30	3.25	1.00	1.00	2,400	88	2,300	2,300	4.5	35.2	32.0
LS305-36	500	36	36	3.25	1.00	1.00	2,160	88	2,300	2,300	4.5	40.2	37.0
LS305-42	500	33	42	3.25	1.00	1.00	1,980	88	2,300	2,300	4.5	45.2	42.0
LS305-48	500	25	48	3.25	1.00	1.00	1,500	88	2,300	2,300	4.5	50.2	47.0
LS310-30	1,000	20	30	3.25	0.50	1.00	2,400	88	5,350	4,250	4.5	35.2	32.0
LS310-36	1,000	18	36	3.25	0.50	1.00	2,160	88	5,350	4,250	4.5	40.2	37.0
LS310-42	1,000	16.5	42	3.25	0.50	1.00	1,980	88	5,350	4,250	4.5	45.2	42.0
LS310-48	1,000	12.5	48	3.25	0.50	1.00	1,500	88	5,350	4,250	4.5	50.2	47.0
LS320-30	2,000	10	30	3.25	0.25	1.00	2,400	88	5,475	3,450	4.5	35.2	32.0
LS320-36	2,000	9	36	3.25	0.25	1.00	2,160	88	5,475	3,450	4.5	40.2	37.0
LS320-42	2,000	8.25	42	3.25	0.25	1.00	1,980	88	5,475	3,450	4.5	45.2	42.0
LS320-48	2,000	6.25	48	3.25	0.25	1.00	1,500	88	5,475	3,450	4.5	50.2	47.0

Front Flange Dimensions

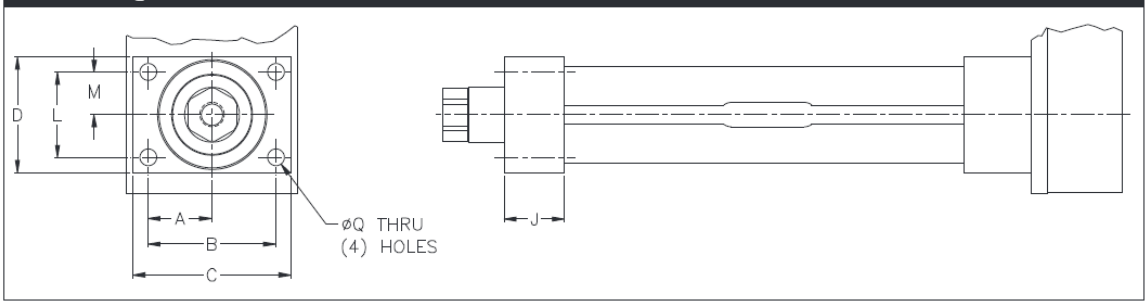

Unit Mounting Dimensions

Model	A	B	C	D	E	F	G	H	J	K	L	M	N	P	Q	R	S	T	U	V	W	X	Y
LS2	1.31	2.63	3.25	2.38	1.19	5/16-18	0.63	6.84	1.00	0.50	1.75	0.88	2.25	0.25	0.34	0.69	1.89	3.78	2.63	5.25	0.50	4.22	1.00
LS3	1.88	3.75	4.50	3.38	1.69	3/8-16	0.75	9.16	1.25	0.50	2.63	1.31	3.25	0.25	0.41	0.94	2.52	5.03	3.50	7.00	0.75	6.28	1.38

SmartMotor™ Series	SM34165MT-IP	
Continuous Torque @ 48V	12.58	lb-in
	201	oz-in
	1.42	N-m
Peak Torque	21.57	lb-in
	345	oz-in
	2.44	N-m
Nominal Continuous Power	448	Watt
	0.45	kW
	0.60	HP
No Load Speed	5,100	V/kRPM
Continuous Current @ Nominal Power	15.5	Amps
Voltage Constant	8.9	V/kRPM
Winding Resistance	0.06	ohms
Encoder Resolution	8000	Counts/Rev
Rotor Inertia	0.0142	oz-in-sec^2
	10.031	10^{-6} kg-m^2
Weight	6.0	lb
	2.72	kg
Shaft Diameter	0.50	in
	12.70	mm
Shaft, Radial Load	30	lb
	13.61	kg
Shaft, Axial Thrust Load	3	lb
	1.36	kg
DeviceNet Version	SM34165MT-IP-DN	
CANopen Version	SM34165MT-IP-C	

All New Class 5 Features and IP65 rated

- Complete barrier against dust and other harmful particles
- Longer motor life
- Splash protected* for wet environments unlike drip-proof competitors
- New industry capabilities such as food and beverage manufacturing and packaging, demanding outdoor conditions, and nautical machinery

* Not submersible

Animatics SmartMotor SM34165MT (No Options) CAD Drawing

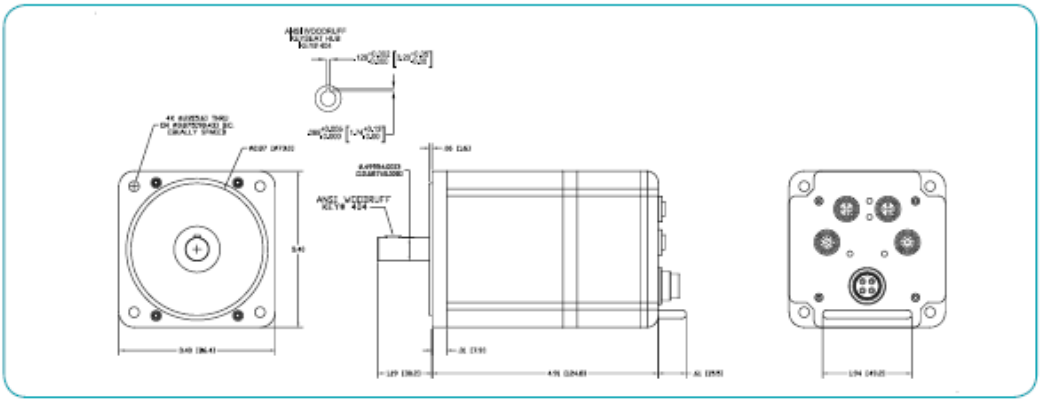

THIS PAGE INTENTIONALLY LEFT BLANK

APPENDIX E

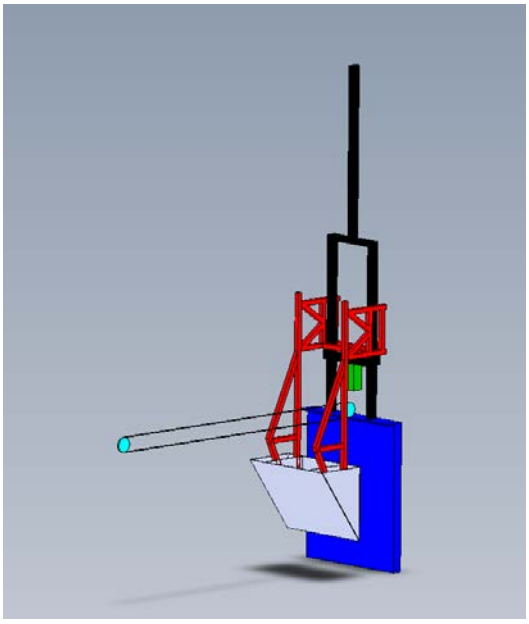

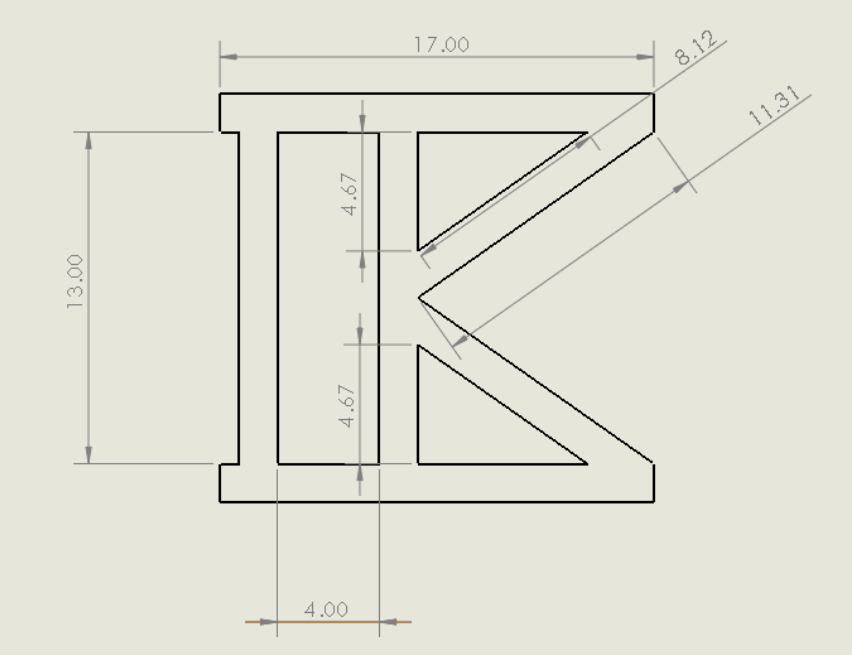

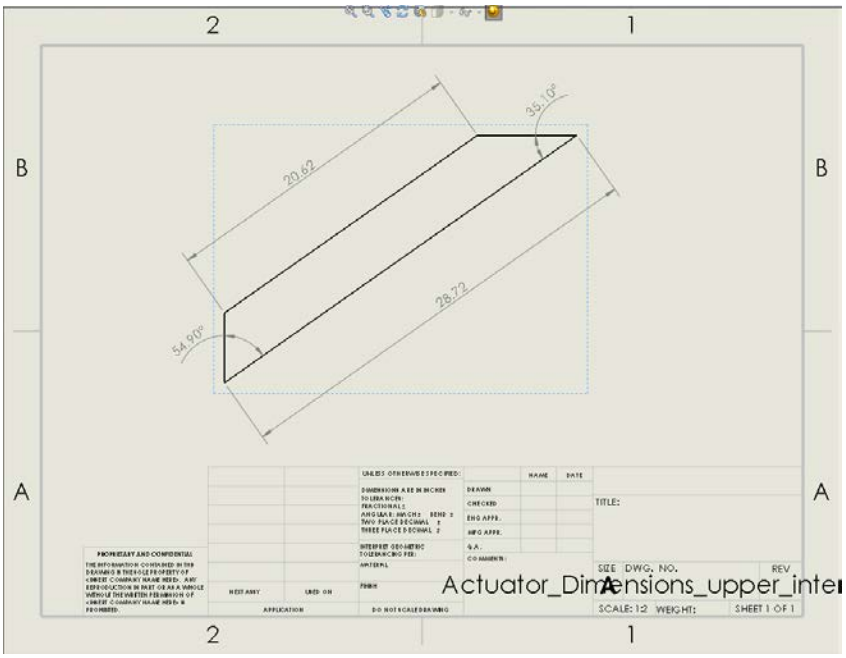
2
1
B
A
20.62
35.10°
28.72
54.90°
Actuator_Dimensions_upper_inter
SCALE: 1:2 WEIGHT:
SHEET 1 OF 1

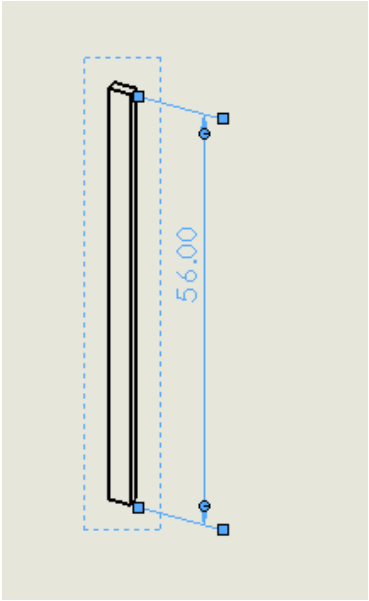
56.00

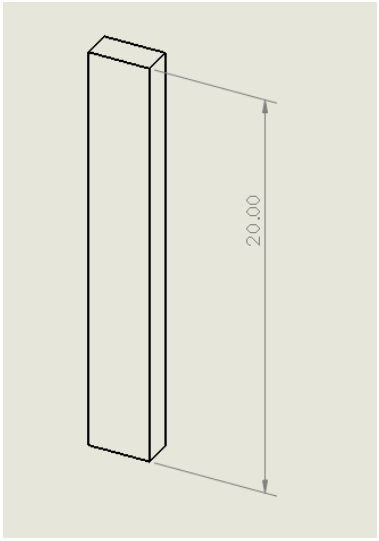
20.00

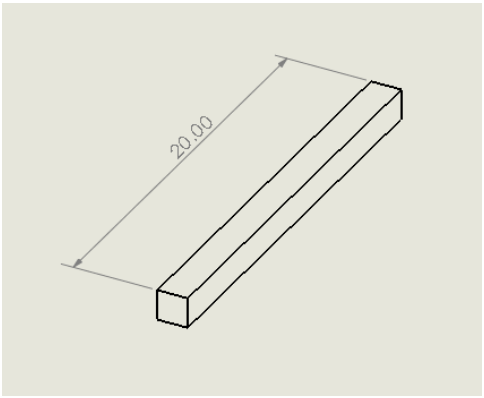
20.00

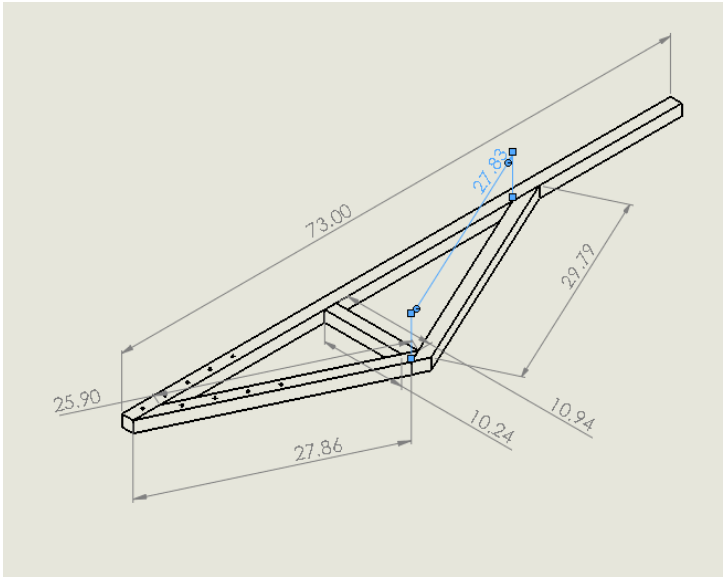
73.00
27.83
29.79
25.90
10.24
10.94
27.86

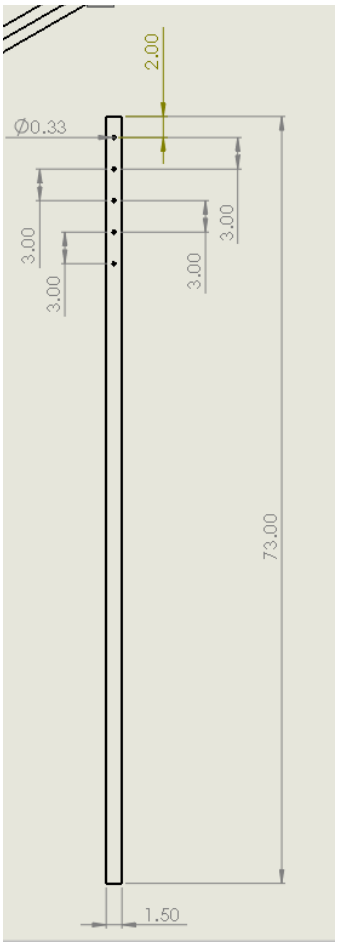
2.00
Ø0.33
3.00
3.00
3.00
3.00
73.00
1.50

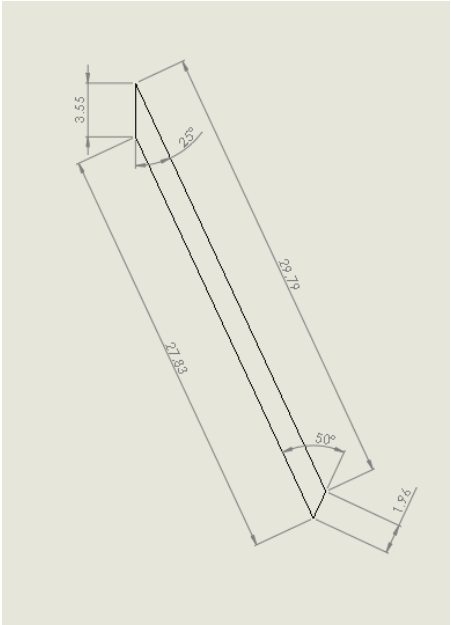
3.55
25°
29.79
27.83
50°
1.96

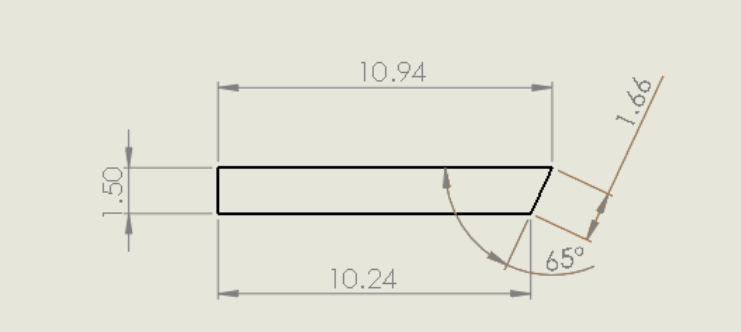
10.94
1.66
1.50
65°
10.24

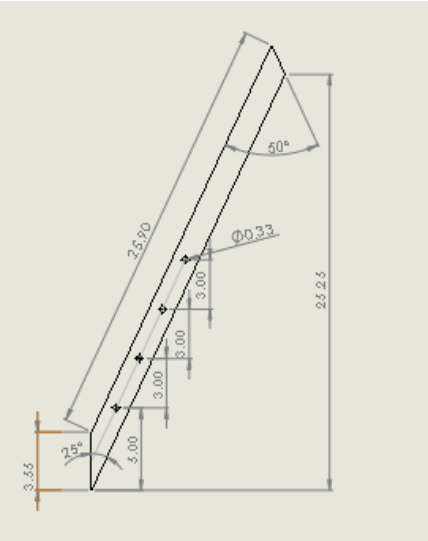
50°
25.90
Φ0.33
3.00
3.00
3.00
5.00
25°
3.55
25.25

Actuator to Stationary Frame Plate

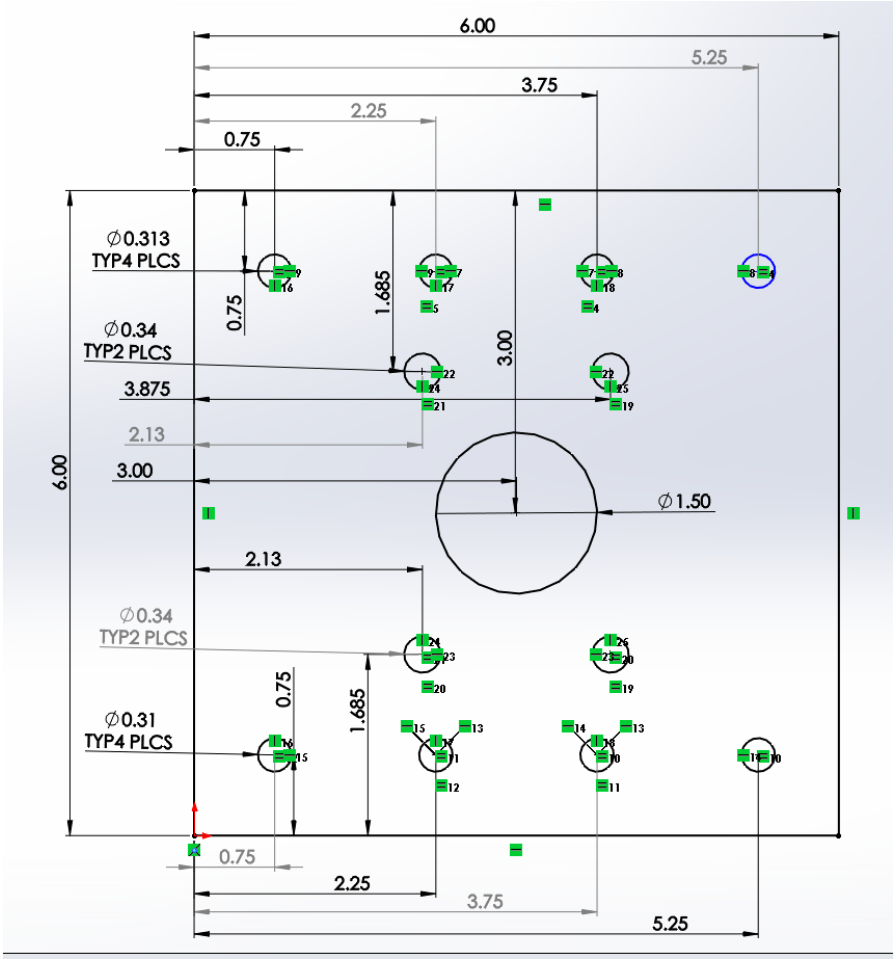

Actuator Frame Plate

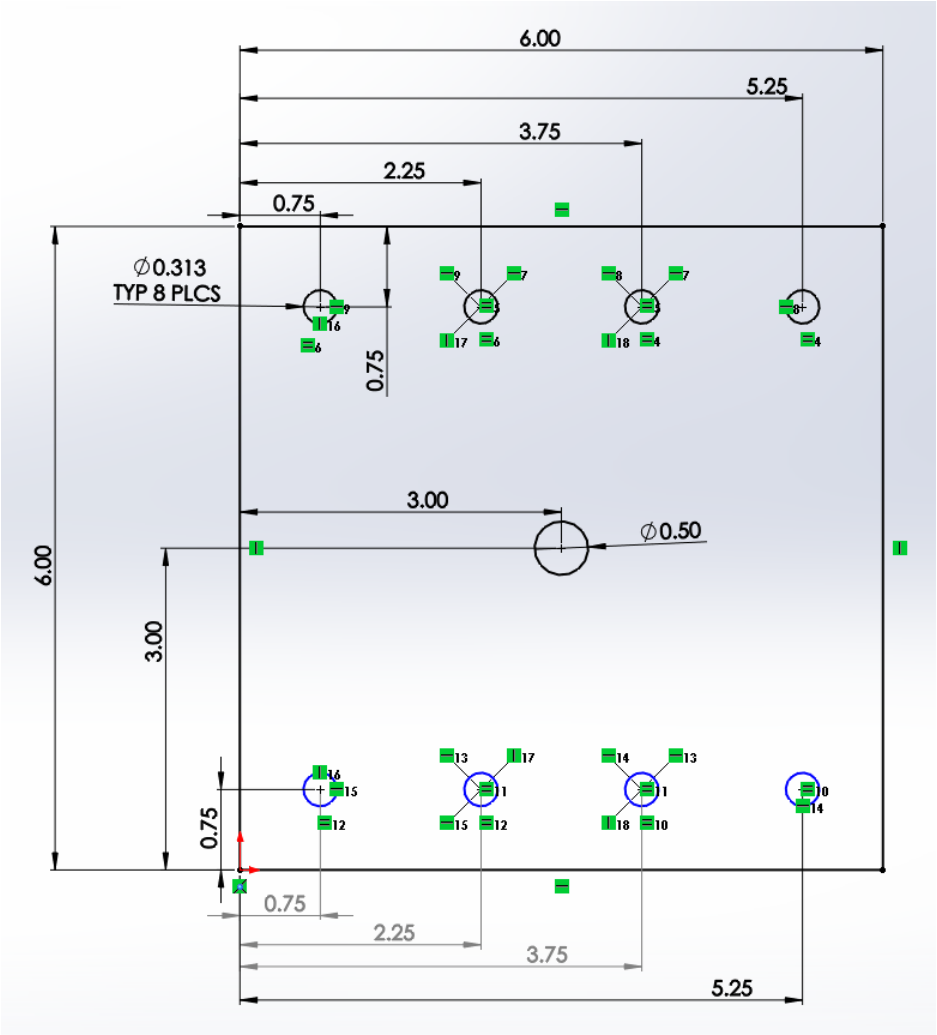

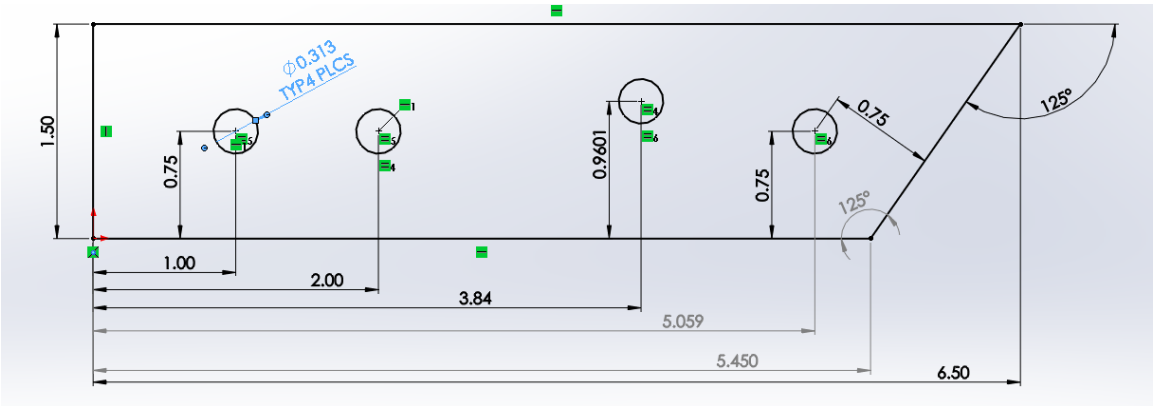

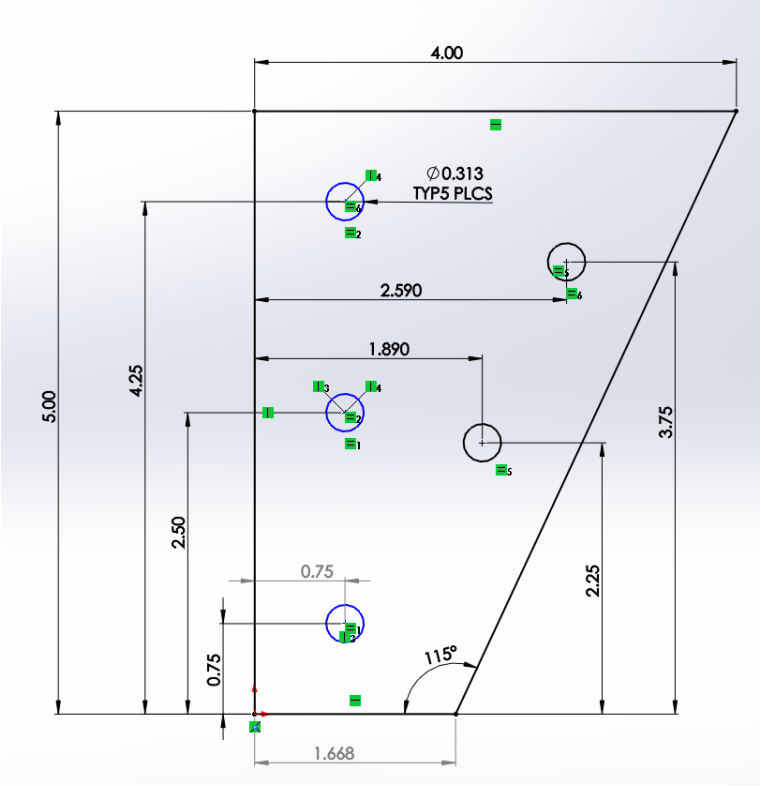
4.00
∅0.313
TYP5 PLCS
2.590
1.890
5.00
4.25
3.75
2.50
2.25
0.75
0.75
115°
1.668

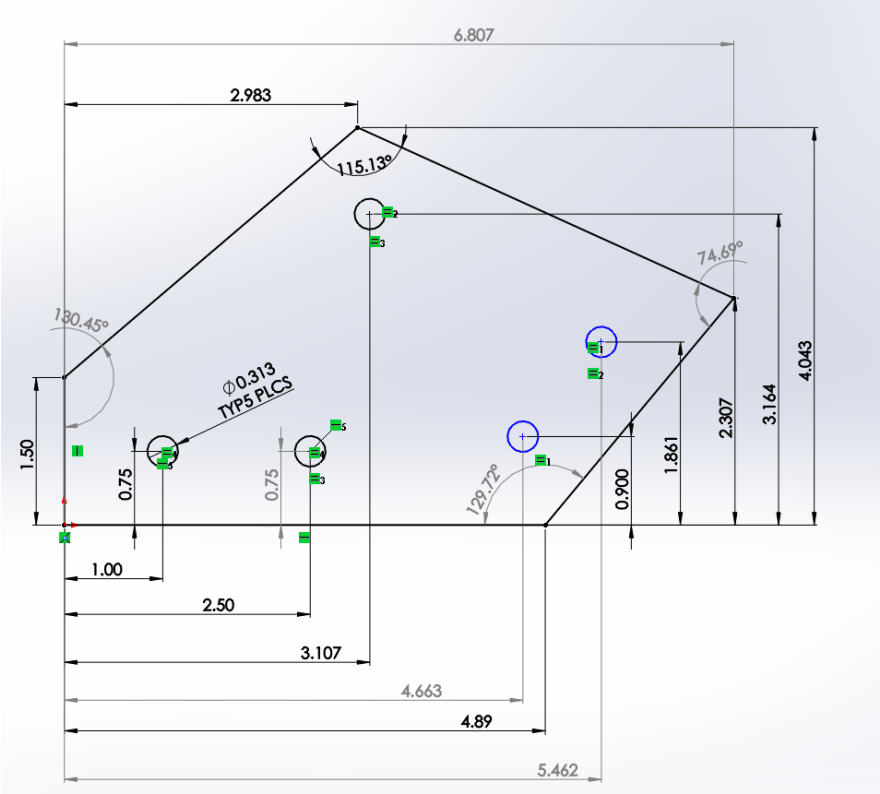
6.807
2.983
115.13°
74.69°
130.45°
∅0.313
TYP5 PLCS
1.50
0.75
0.75
129.72°
0.900
1.861
2.307
3.164
4.043
1.00
2.50
3.107
4.663
4.89
5.462

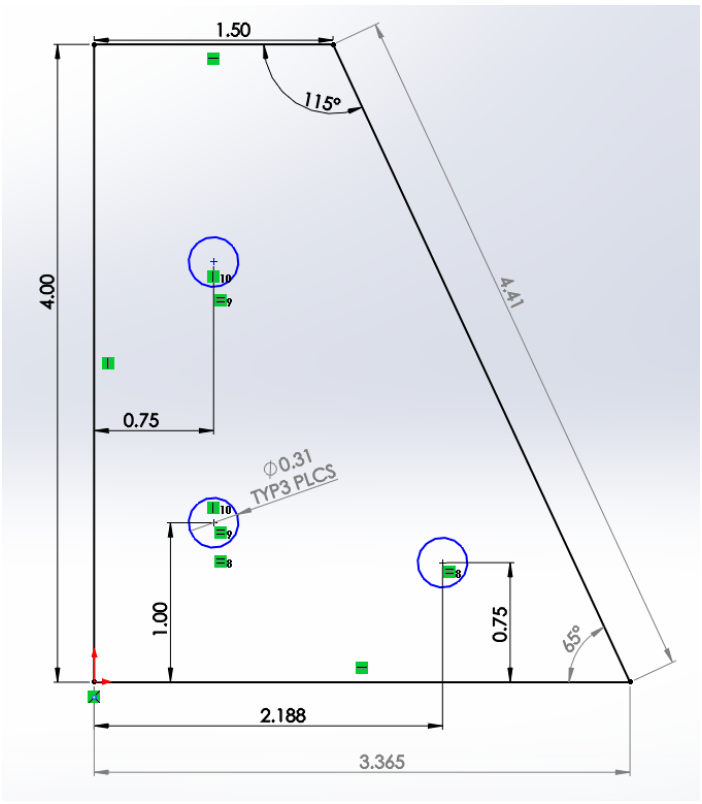
1.50
115°
4.00
4.41
0.75
∅0.31
TYP3 PLCS
1.00
0.75
65°
2.188
3.365

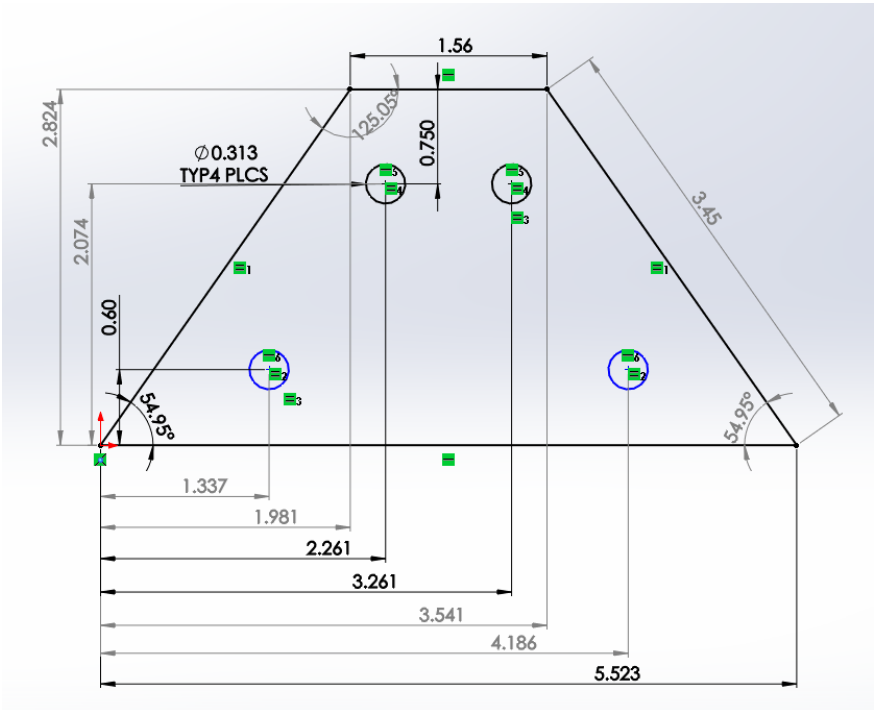
1.56
125.05°
2.824
∅0.313
TYP4 PLCS
0.750
3.45
2.074
0.60
54.95°
54.95°
1.337
1.981
2.261
3.261
3.541
4.186
5.523

THIS PAGE INTENTIONALLY LEFT BLANK

LIST OF REFERENCES

[1] H. Lindstad, "Economic Savings Linked to Future Arctic Shipping Trade are at Odds with Climate Change Mitigation," *Transport Policy*, vol. 45, pp. 24–30, Sep. 2015.

[2] C. Mooney. (2015, Sep. 10). "*The Arctic is melting –but shipping through the Northwest Passage is another story*." [Online]. Available: https://www.washingtonpost.com/news/energy-environment/wp/2015/09/10/why-the-northwest-passage-probably-wont-be-ready-for-shipping-any-time-soon/. [Accessed 8 January 2016].

[3] C. Haas, "*Ice Thickness in the Northwest Passage*," Geophysical Research Letters, AGU Journal, 2015. [Online]. Available: http://onlinelibrary.wiley.com/doi/10.1002/2015GL065704/full. [Accessed 5 December 2015].

[4] The k2p blog. (2014, January 26.) Re: The Real Interests in the Arctic. Retrieved from https://ktwop.com/tag/territorial-claims-in-space/. [Accessed 12 January 2016].

[5] Arctic Council. (2016, May 13). "*The Arctic Council: A Backgrounder.*" [Online]. Available: http://www.arctic-council.org/index.php/en/about-us. [Accessed 12 January 2016].

[6] S. L. Myers, "Arctic Council Adds 6 Nations as Observer States, Includiing China," The New York Times, 15 May 2013. [Online]. Available: http://www.nytimes.com/2013/05/16/world/europe/arctic-council-adds-six-members-including-china.html?_r=0. [Accessed 12 January 2016].

[7] Department of Defense, "Arctic Strategy," Secretary of Defense, 2013. [Online]. Available: http://archive.defense.gov/pubs/2013_Arctic_Strategy.pdf. [Accessed 12 January 2016].

[8] Defence IQ Press, "U.S. Navy Conducts ICEX Exercise in Arctic, Reinforcing Strategic Importane of Region," Defence IQ Press, 25 March 2014. [Online]. Available: http://www.defenceiq.com/naval-and-maritime-defence/articles/u-s-navy-conducts-icex-exercise-in-arctic-reinforc/. [Accessed 12 January 2016].

[9] D. McKinney, "Navy Research Look to Rotating Detonation Engines to Power the Future," U.S. Naval Research Laboratory, 2 November 2012. [Online]. Available: http://www.nrl.navy.mil/media/news-releases/2012/Navy-Researchers-Look-to-Rotating-Detonation-Engines-to-Power-the-Future. [Accessed 12 January 2016].

[10] P. Rossetti, “Challenges to the Navy in the Arctic Region,” American Security Project, 22 January 2015. [Online]. Available: http://www.americansecurityproject.org/challenges-to-the-navy-in-the-arctic-region/. [Accessed 12 January 2016].

[11] S. Bolstad, “Hydrodynamic Response of a Composite Structure in an Arctic Environment,” M.S. thesis, Dept. Mech. Aerosp. Eng.,Naval Postgraduate School, Monterey, 2015.

[12] NavSource, “USS Zumwalt (DDG-1000),” Paul R. Yarnall and NavSource Naval History, 2013. [Online]. Available: http://www.navsource.org/archives/05/011000.htm. [Accessed 12 January 2016].

[13] J. Judson, “The Icebreaker Gap,” Politico, 1 September 2015. [Online]. Available: http://www.politico.com/agenda/story/2015/09/the-icebreaker-gap-000213. [Accessed 12 January 2016].

[14] R. Tiron. (2004, Jul.). “*Navy Gradually Embracing Composite Materials in Ships*.” [Online]. Available: http://www.nationaldefensemagazine.org/archive/2004/July/Pages/Navy_gradually3506.aspx. [Accessed 10 January 2016].

[15] Navy Technology, “M80 Stiletto Mission Scenario,” Kable, 2016. [Online]. Available: http://www.naval-technology.com/projects/m80-stiletto/. [Accessed 10 January 2016].

[16] D. K. Park, “Operability of Non-Ice Class Aged Shops in the Arctic Ocean -Part 1: Ultimate Limit State Approach,” Elsevier Ocean Engineering, 2015. [Online]. Available: http://www.sciencedirect.com/science/journal/00298018/102/supp/C [Accessed 11 January 2016].

[17] M. F. Pinnell and P. O. Sjoblom, “Low-velocity impact testing of thermoplastic,” Wright Res. and Dev. Cent. AF Sys. Comm., Wrigh-Patterson AFB, 1990.

[18] A. C. Owens, “Failure Mechanics in Low-Velocity Impacts on Thin Composite Plates,” Langley Res. Cent., Hampton, 1983.

[19] J.-H. Kim, “*Safety Assessment of Cargo Containment Systems in LNG Carriers Under the Impact of Iceberg-Ship Collision*,” ASME 30th International Conference on Ocean, Offshore, and Arctic Engineering, Rotterdam, NL. 2011, vol. 1, pp. 975-982.

[20] C. Daley, “*Ice Collision Forces Considering Structural Deformation*,” ASME 29th Internation Conference on Ocean, Offshore and Arctic Engineering, Shanghai, CN. 2010, vol. 4, pp. 817–825.

[21] Naval Surface Warfare Center Indian Head Division, DYSMAS User’s Manual, Indian Head: Naval Surface Warfare Center, 2013.

[22] J. A. Wardlaw, J. R. Luton, K. C. Renzi and R. M. Kiddy, The Gemini Euler Solver for the Coupled Simuation of Underwater Explosions, Indian Head: NSWC Indian Head, 2003.

[23] E. Schulson, “The Structure and Mechanical Behavior of Ice,” The Minerals, Metals & Materials Society, 1999. [Online]. Available: http://www.tms.org/pubs/journals/JOM/9902/Schulson-9902.html. [Accessed 11 January 2016].

[24] United States Army Corps of Engineers, “Coastal Engineering Mannual,” Vicksburg, USACE, 2006, p. 69.

[25] Boundless, “Superposition and Interference,” [Online]. Available: https://www.boundless.com/physics/textbooks/boundless-physics-textbook/waves-and-vibrations-15/wave-behavior-and-interaction-126/superposition-and-interference-444-6329/. [Accessed 2 February 2016].

[26] T. Sarpkaya and M. Isaacson, Mechanics of Wave Forces on Offshore Structures, New York: Van Nostrand Reinhold Company, 1981.

[27] A. Lavrov and C. G. Soares, “CFD Modelling of the Waves Generated by a Wedge-Shaped Wave Maker,” *Research Gate*, p. 2, 2015.

[28] K. Tanizawa and M. Minami, “Wave Tank,” Ship Research Institute, Japan, 2000. [Online]. Available: http://www.isope.org/conferences/numericalwavetank/WaveTank/nwtws2000/EXP.htm. [Accessed 2 February 2016].

[29] Edinburgh Designs, “Wave Generators,” Edinburgh Designs, 2016. [Online]. Available: http://www.edesign.co.uk/waves/some-wave-1/. [Accessed 15 November 2015].

[30] J. Zseleczky, Interviewee, *Naval Academy Sediment Tank*, [Interview]. 10 September 2015.

[31] Y.-C. Jeon, “Scotch Yoke Mechanism,” GrabCad, 11 April 2013. [Online]. Available: https://grabcad.com/library/scotch-yoke-mechanism—2. [Accessed 10 November 2015].

[32] T. Balcezak, Interviewee, *E-Drive Acutator*. [Interview]. 26 January 2016.

[33] OnlineMetals.com, “Aluminum Bare Sheet 6061 T6,” Online Metals, 2016. [Online]. Available: http://www.onlinemetals.com/merchant.cfm?pid=1247&step=4&showunits=inches&id=76&top_cat=60. [Accessed 4 December 2015].

[34] S. M. Arbogast, “The Influence of Shock-Induced Air Bubble Collapse Resulting From Underwater Explosive Events,” M.S. thesis, Dept. Mech. Aerosp. Eng., Naval Postgraduate School, Monterey, 2012.

THIS PAGE INTENTIONALLY LEFT BLANK

INITIAL DISTRIBUTION LIST

1. Defense Technical Information Center
   Ft. Belvoir, Virginia

2. Dudley Knox Library
   Naval Postgraduate School
   Monterey, California